BABEȘ-BOLYAI UNIVERSITY
Faculty of Chemistry and Chemical Engineering

Summary

Modelling approaches for thermo-chemical gas-solid systems applied to energy conversion processes with carbon dioxide capture

PhD Candidate: Eng. Sandu Vlad-Cristian
Supervisor: Prof. PhD Eng. Cormoș Călin-Cristian

Cluj-Napoca, 2021

Summary table of contents

Thesis table of contents

Keywords

calcium looping; carbon dioxide capture and storage; chemical looping combustion; computational fluid dynamics modelling; hydrogen production; process flow modelling; sorption-enhanced water-gas shift.

1. Introduction

1.1. Motivation and background

The presence of greenhouse gases (GHG) in the atmosphere is essential to life on earth as it causes the greenhouse effect, which contributes to the natural warming of the surface by trapping heat from the sun that would otherwise escape back into space. However, higher concentrations of GHGs in the atmosphere lead to additional heat being trapped, rising global temperature levels [1].

The major anthropogenic GHG is CO_2, accounting for 76% of total anthropogenic GHG emissions in 2010 [2]. Most CO_2 emissions come from fossil fuel combustion and industrial processes, as illustrated in Figure 1.

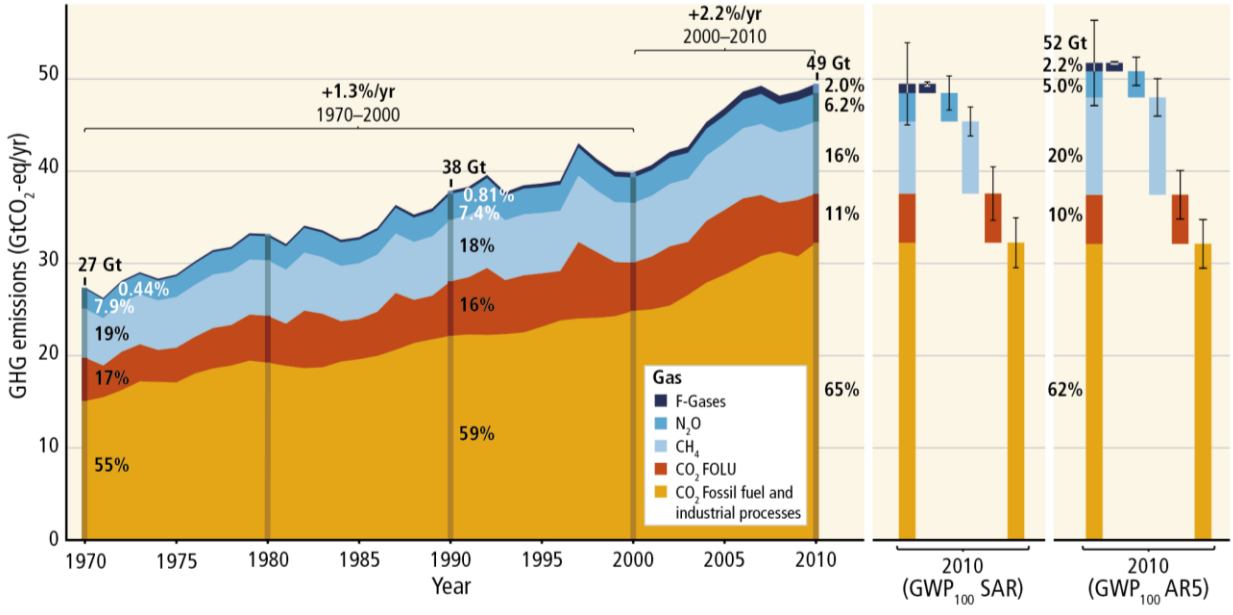

Figure 1. Total annual anthropogenic GHG emissions by gases 1970-2010 [2]

Aside from CO_2 emissions resulting as a consequence of electricity and heat production, the industrial sector is also a primary contributor to global emissions [3]. Industry related CO_2 emissions are mainly due to combustion of fossil fuels on site used at facilities for energy generation [4,5].

Only production of iron and steel, representing 22% of total industrial energy usage, and other non-metallic minerals, mostly cement with 7% energy consumption, accounted for 55% of all CO_2 emitted (direct, indirect and process-based) from industry, as reported by the International Energy Agency (IEA) for 2014 [6,7]. The largest industrial consumers of energy was the chemical and petrochemical one, representing 28% of all industry related energy utilization, with the third most CO_2 emissions at 13%,

behind steelmaking and cement production processes [8]. Production of aluminium was small when compared to steel, consuming only 4% of industrial energy consumption, and was primarily associated with a high demand in electricity, with indirect emissions causing more than 80% total CO_2 emissions when considering the aluminium production process [9]. Finally, pulp and paper production were responsible for 4% energy consumption of the industrial sector, fuel and energy usage being primary sources of CO_2 during all stages (i.e., forestry, pulping and manufacturing) of production [6].

Industry related emissions, representing around 24% of worldwide GHG emissions in 2016 [3], are expected to increase, as global economic recovery will lead to higher energy demand, surpassing pre-Covid-19 levels [10]. Alongside heat and power generation, it is necessary to also decarbonise the industry sector in order to avoid new highs in CO_2 emissions and curb a rebound in emissions.

Lower emissions associated with the power sector can be achieved by decarbonisation and improved energy efficiency. Ideally, a switch from fossil fuel-based energy production to energy production using non-fossil and other renewable sources would lead to the essential outcome of net zero CO_2 emissions, but the electricity demanded by ongoing economic growth cannot be currently provided solely by relying on renewable energy sources due to their fluctuating nature. Moreover, developing countries depend on low-cost fossil fuel-based energy production and cannot justify the resources required to replace their existing power plants [11]. During this unavoidable transition period to renewable energy sources, fossil fuels will continue to be the dominant global energy source [12]. Consequently, measures to improve the energy sector and reduce greenhouse gas emissions have been assessed by the Intergovernmental Panel on Climate Change (IPCC) [4].

A solution that enables the continuation of fossil fuel usage, while mitigating CO_2 emissions, is carbon capture and storage (CCS). CCS is the process through which CO_2 is captured at large emission sources, such as power plants or industrial processes. The separated CO_2 is then transported to a storage site and injected into rock formations for permanent storage or depleted oil/gas reservoirs to enhance oil recovery. Instead of being stored, the captured CO_2 can be used as feedstock to produce methanol, urea or synthetic fuel [13].

The IPCC [14] outlines three main approaches to applying CCS technologies, shown in Figure 2, depending on the power plant or process in question:

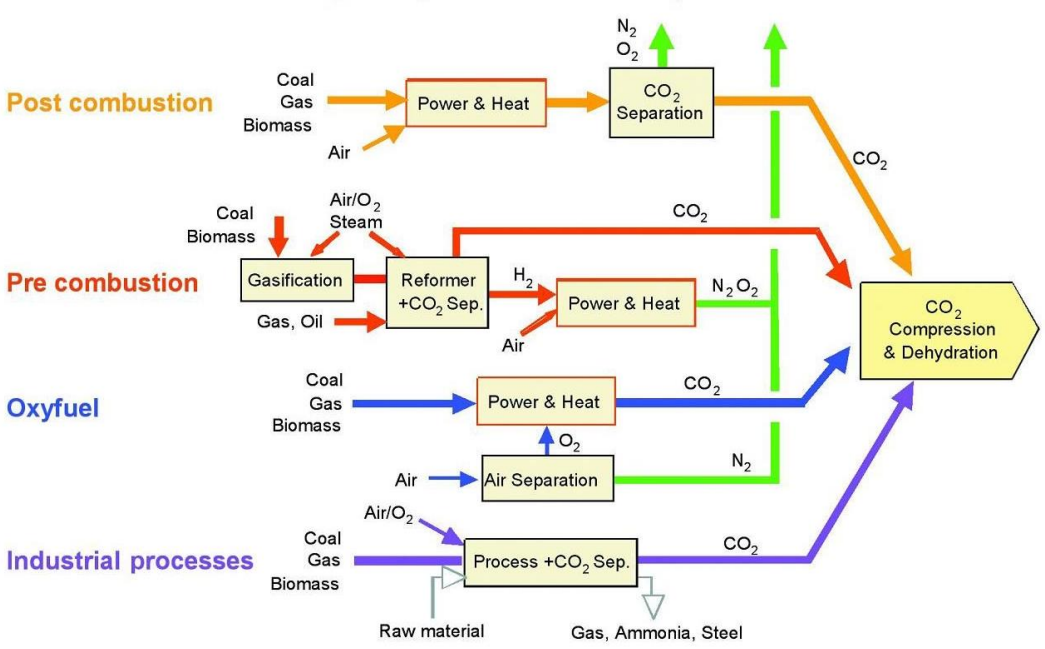

Figure 2. Overview of CO_2 capture processes and systems [14]

- Post-combustion systems capture CO_2 from the flue gases produced following fossil-fuel combustion in air. The flue gases, instead of being released straight into the atmosphere, are passed through equipment to carry out CO_2 separation. Post-combustion systems can be applied to any type of fuel, but accounting for fuel impurities is paramount in achieving a cost-efficient design of the final plant [15]. The most commonly seen method in post-combustion capture is through absorption with liquid solvents in order to separate the small fraction of CO_2 and nitrogen from the flue gas stream. The absorption process based on chemical solvents is preferred due to the high level of capture efficiency and selectivity. For modern pulverized coal (PC) or natural gas combined cycle (NGCC) power plants, monoethanolamine (MEA) is the most utilized organic solvent in post-combustion capture systems. The MEA-based CO_2 capture technology is considered a performance benchmark among other carbon capture applications [16].
- Pre-combustion systems capture CO_2 prior to fuel combustion. The primary fuel is processed in a reactor with steam and air/oxygen to produce syngas, a mixture of carbon monoxide and hydrogen. Syngas generation is mainly achieved through two ways; the first approach is by adding steam to the primary fuel (Eq. (1)), leading to a process called steam reforming, while the second method is by adding oxygen to the fuel (Eq. (2)), known as partial oxidation when applied to fluid fuels and gasification when applied to solid fuels.

$$C_xH_y + xH_2O \rightleftarrows xCO + (x + y/2)H_2 \quad (1)$$

$$C_xH_y + x/2\,O_2 \rightleftarrows xCO + (y/2)H_2 \quad (2)$$

A second reactor, called shift reactor, is used to convert carbon monoxide from the syngas and steam into additional hydrogen and carbon dioxide through the water-gas shift (WGS) reaction. Thus, separate streams of hydrogen and carbon dioxide can be obtained. Pre-combustion systems are most suitable for integrated gasification combined cycle (IGCC) power plants.

- Oxyfuel combustion systems use pure oxygen instead of air when combusting fuel. As a result, the flue gas is comprised of mainly high concentrations of CO_2 and water vapour. The CO_2 can be easily separated by condensing the water vapour from the gas stream, resulting in a stream of 80% - 98% CO_2 depending on type of fuel combusted with impurities such as NO_x, SO_x, HCl and Hg. A major drawback of oxyfuel combustion systems is the energy intensive requirement of an air separation unit (ASU), necessary to obtain pure oxygen, incurring an energy penalty of around 7% - 10% [17].

While not all thermal power plant systems are compatible with every capture method (i.e., only pre-combustion can be employed in IGCC, post-combustion and oxy-combustion can fit PC and all three methods can be applied to NGCC), costs related to CO_2 capture plants for power generation, regardless of applied technology, can be estimated by using various economic metrics, such as capital cost, electricity cost, CO_2 avoided cost and cost to capture CO_2.

1.2. WGS and SEWGS technologies

1.2.1. Water-gas shift reaction

WGS is a reversible reaction (Eq. (3)) through which CO and H_2O are converted to produce H_2 and CO_2. The oxygen from the H_2O molecule will transfer to CO and transform into CO_2, while the H_2O will become the source to produce H_2:

$$CO + H_2O \rightleftarrows CO_2 + H_2 \qquad \Delta H^0_{298} = -41\ kJ \cdot mol^{-1} \quad (3)$$

WGS is an essential part of various reactions encountered in industry (e.g., steam reforming [18], partial oxidation [19], autothermal reforming [20], gasification [21], methanol and dimethyl ether syntheses [22], Fischer-Tropsch process [23], ironmaking in a blast furnace [24], etc.).

The reversible reaction is moderately exothermic, typically driven by the presence of various catalysts. The behaviour of the WGS reaction is equilibrium-controlled and heavily dependent on temperature.

Equilibrium is not affected by pressure, since the number of moles does not change when WGS occurs, but total pressure enhances reaction rate and positively influences CO conversion [25].

Theoretically, the presence of CO and H_2O in a system should trigger the WGS reaction, however, the reaction does not occur at low temperatures because of the WGS energy barrier. Therefore, it is mandatory to use catalysts in order to achieve a reduction of the activation energy and overcome the WGS energy barrier. Depending on which catalyst is being used and reaction temperature, the WGS can be classified as high-temperature shift (HTS) at temperatures ranging from 300℃ - 500℃ or low-temperature shift (LTS) between 150℃ - 250℃.

The Arrhenius Law states that reaction rate is promoted with increasing temperature, while Le Chatelier's principle reveals that lower temperatures improve CO conversion (i.e., higher H_2 yield), meaning HTS is driven by reaction kinetics and thermodynamic equilibrium dominates the LTS [26]. As a way to suppress WGS equilibrium limitations and achieve a higher conversion of CO, the WGS reaction is carried out at the industrial scale in separate stages using two adiabatic reactors arranged in series. Initially, the HTS takes place with the purpose to generate hydrogen, after which a LTS reaction maximizes the CO conversion. Finally, separation of CO_2 and H_2 is accomplished with energy intensive processes, such as solvent absorption or pressure swing adsorption (PSA) [27].

When combining WGS with CCS, the most promising technology for pre-combustion and post-combustion carbon capture is sorption-enhanced water-gas shift (SEWGS). Moreover, the technology can be utilized to reduce carbon in syngas produced with coal-based feedstock, improving the concentration of hydrogen in the product stream [28]. The WGS reaction and subsequent CO_2 separation are essential in an IGCC process for electricity production with CO_2 capture [29].

1.2.2. Sorption-enhanced water-gas shift process

Separation of products applied to the WGS reaction pushes the equilibrium to the right, according to Le Chatelier's principle, leading to better reaction performance and a high purity hydrogen stream. SEWGS is a pre-combustion technology with great potential that combines the WGS reaction (Eq. (3)) with in-situ adsorption of CO_2 (Eq. (4)) at high-temperatures between 300℃ - 500℃ and high-pressure levels between 10 bar - 40 bar. Steam adsorption (Eq. (5)) is also possible based on process conditions.

$$CO_2 + \bullet \rightleftarrows CO_2 - \bullet \quad (4)$$

$$H_2O + \bullet \rightleftarrows H_2O - \bullet \quad (5)$$

Conventional WGS technology requires two consecutive reactors to obtain high conversion of CO, followed by PSA to separate the CO_2 from the pure H_2, whereas with SEWGS, the second reactor and PSA

can be combined into a SEWGS unit, leading to less process steps and less equipment needed (Figure 3). Moreover, in the case of a steam methane reformer without carbon capture, the CO_2 is released into the atmosphere, while SEWGS enables high CO_2 capture ratios at a higher energy efficiency and lower cost in comparison with more mature technologies [30].

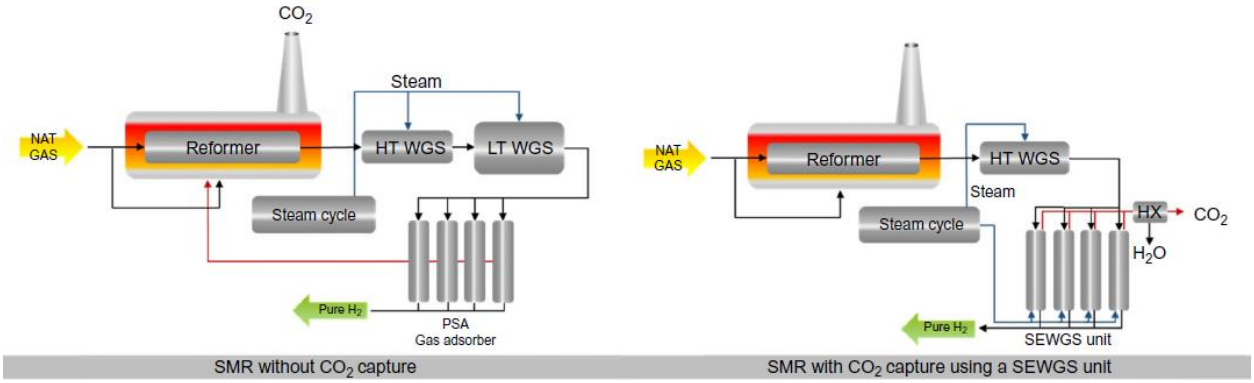

Figure 3. Conventional steam methane reforming (SMR) (left) and with carbon capture SEWGS integration (right) [31]

Considerable efforts were made in testing different sorbents to be used in a SEWGS process, however, most proved to be less desirable for various reasons. Hydrotalcite based adsorbents seem to outclass other types of adsorbents, as they demonstrate high thermal stability, fast sorption kinetics and high CO_2 selectivity [32,33]. The most commonly known hydrotalcite is Mg-Al HTC.

The potassium-promoted hydrotalcite (K-HTC) has two crucial roles, acting as catalyst for the WGS reaction and sorbent for reversibly adsorbing CO_2. After adsorption, the CO_2 that is released during K-HTC regeneration, is sufficiently pure to be stored [34,35].

A SEWGS process (Figure 4) involves a series of reactors which run in pressure cycles, enabling the periodic loading and regeneration of the sorbent. Since multiple reactors are being used, the process acts as if continuous and leads to a constant production of separate streams of CO_2 and H_2.

In the first cycle step, syngas enters the column in which CO reacts with steam to obtain CO_2 and H_2. CO_2 is taken up by adsorption and a H_2 rich stream is obtained. Once the sorbent is saturated, a medium-pressure steam rinse takes place pushing the syngas into another reactor. After the rinse, a number of pressure equalizations are performed. During this step, the rinse gas in the high-pressure reactor expands and pushes the remaining syngas into a lower pressure reactor. Gas pressure is conserved since the high-pressure reactor that required depressurization will connect to a lower pressure one that needs to be pressurized. In the blowdown step, the pressure in the reactor is rapidly decreased to 1 bar and some CO_2 is released from the sorbent, exiting the reactor with the steam and allowing particle regeneration. By purging the reactor with low-pressure steam, additional CO_2 is released and sorbent regeneration is

enhanced. Following pressure equalization with a high-pressure reactor and re-pressurization, the reactor will be ready to undergo the SEWGS process from the beginning.

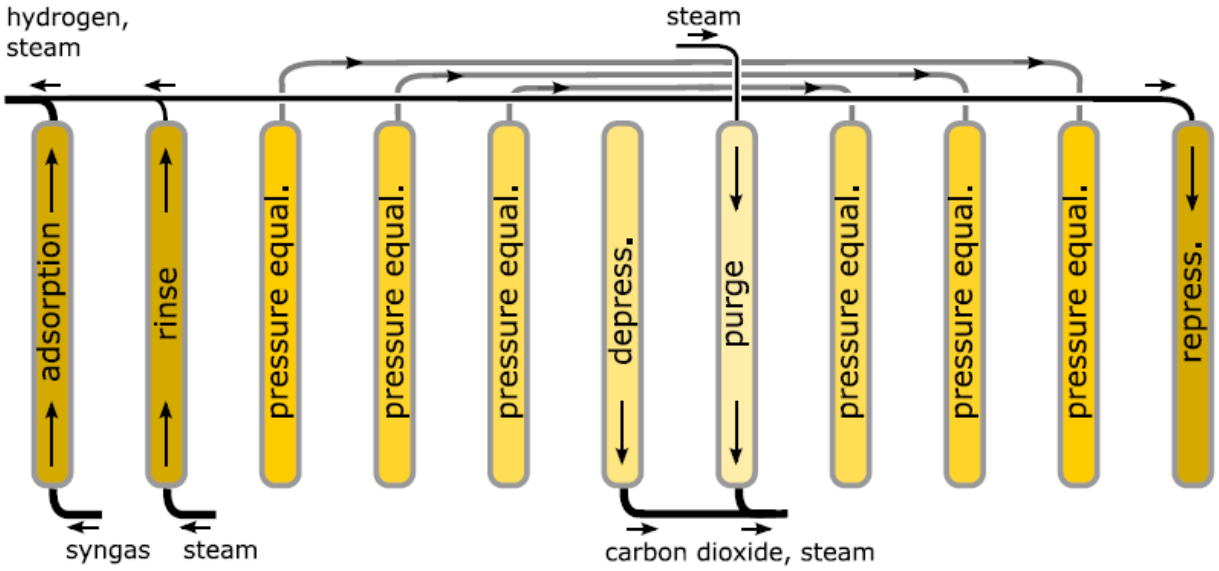

Figure 4. Eleven step SEWGS cycle with concurrent steam rinse [36]

SEWGS is an attractive process for both pre-combustion CCS and GHG emissions reduction since it directly converts syngas into a hot H_2 stream at feed pressure and a separate CO_2 stream at regeneration pressure [36–38].

1.3. Chemical looping technologies

In chemical looping (CL), air is not used in the combustion reaction and the oxygen is provided via an oxygen carrier (OC) undergoing a continuous redox cycle, thus preventing dilution of the flue gases with nitrogen. One advantage of CL over conventional oxy-combustion is circumventing the need for an ASU to provide oxygen for combustion [39]. The CL technology can be categorized into subprocesses such as chemical looping combustion (CLC), chemical looping hydrogen (CLH), chemical looping gasification (CLG) and OC aided combustion (OCAC), with respect to oxygen source (i.e., H_2O and/or air) and desired process output (syngas, H_2, CO_2).

CLC is an alternative to conventional combustion, where a solid oxygen carrier, usually a metal oxide, is integrated into the combustion reaction in order to supply the oxygen required for fuel conversion. If the fuel is completely oxidized, the resulting stream will be a mixture of steam and high concentration of CO_2. The captured CO_2 can be sent to storage or utilization after H_2O condensation. Following OC depletion, regeneration takes place by supplying air or steam, depending on the desired output [40], i.e., air will be

used for OC reoxidation for heat and power generation in a CLC process, while steam will be used for hydrogen production in chemical looping reforming (CLR) or CLH processes [41]. The heat released as a result of the redox steps within CLC is the same amount of energy as in the case of regular combustion, as stated by Hess's law, i.e., the net enthalpy change seen in the full reaction does not change, regardless of the number of steps necessary to complete the reaction [42].

The fuels utilized in combustion can be either gaseous or solid. For gaseous fuels, the metal-based OC react with fuels (i.e., natural gas, refinery gas) to obtain a stream of CO_2 and H_2O. During combustion, the OC is reduced, but will undergo regeneration during the oxidation step. The CO_2 can be separated by condensing the water, with no additional energy required to produce high purity CO_2.

Conventionally, CLC utilizes a circulating fluidized bed configuration (CFB) in which the OC is circulated between two separate reactors, a fuel and an air reactor (Figure 5), with reduction (Eq. (6)) taking place in the fuel reactor and oxidation (Eq. (7)) in the air reactor [43]. The reactor concept was proposed by Lyngfelt et al. [44] in 2001 and comprised of an air reactor or riser, cyclone and fluidised bed. Air and fuel will never come into contact since the two reactors are independent, meaning separation of CO_2 from N_2 is inherently circumvented. Selecting the proper OC with desirable properties (i.e., high oxygen transport capacity, high CO_2 selectivity, superior mechanical strength, high reactivity) is paramount in the development of an interconnected fluidised bed. The advantages that enabled the CFB to become the main configuration seen in CLC are decent solid-gas mixing, low pressure drop, homogeneous temperature and efficient heat transfer [45], as well as the innate characteristic to be applied to continuous processes. As consequences of the high velocities used in CFB configurations, equipment erosion and attrition of solids can occur [46].

$$(2n+m)Me_xO_y + C_nH_{2m} \rightarrow (2n+m)Me_xO_{y-1} + nCO_2 + mH_2O \quad (6)$$

$$2Me_xO_{y-1} + O_2 \rightarrow 2Me_xO_y \quad (7)$$

where Me_xO_y and Me_xO_{y-1} are the oxidized and reduced forms of the OC and C_nH_{2m} is the fuel.

A packed bed reactor concept for CLC was published by Noorman et al. [47]. The single reactor contains the OC particles which undergo the oxidation and reduction steps in alternation by switching the gas feed composition to fuel and air. The packed bed configuration enables process operation at high pressures, a significant advantage over the conventional CFB reactors. The main challenges consist of supplying high temperatures and providing a gas controlling system for high flow rates. The fixed bed reactor design utilized for CLC of syngas is investigated in Chapter 4, following a detailed comparison of packed bed versus traditional CFB configurations.

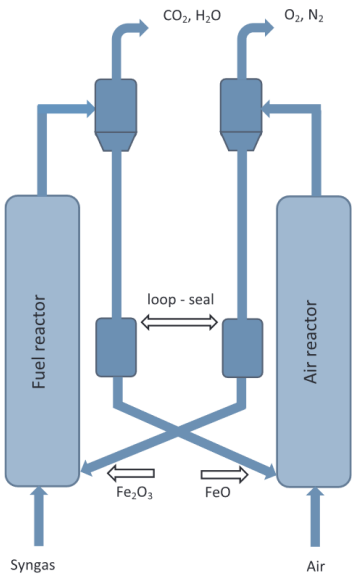

Figure 5. Diagram of CLC of syngas using an interconnected fluidized bed configuration with iron-based OC [43]

The successful operation of a CL process depends on the OC material used. Ideally, the OC should be cost-efficient and highly reactive, with a high melting point, high oxygen transfer capacity, low tendency of agglomeration and low particle attrition to enable operation of multiple cycles [48]. Although less reactive and with lower thermal and mechanical stability than synthetic OCs, natural mineral-based OCs are often chosen due to their economic benefits.

Calcium looping (CaL) makes use of the reversible carbonation-calcination process as an option for both pre-combustion and post-combustion CO_2 capture. In the post-combustion configuration (Figure 6), fuel combustion takes place with air and the resulting flue gas enters the carbonator where the direct reaction seen in Eq. (8) occurs. The CO_2 is sent to the calciner as $CaCO_3$ and the carbon-free flue gas leaves the carbonator. In the calciner, the endothermic decomposition of $CaCO_3$ back into CaO and CO_2 takes place with the energy provided by an oxy-combustion process. A pure CO_2 stream is obtained and ready to be stored or used in other processes [49].

$$CO_2 + CaO \rightleftarrows CaCO_3 \qquad \Delta H^0_{298} = -183\ kJ \cdot mol^{-1} \qquad (8)$$

The CaL process is generally carried out using a dual fluidized bed system to promote contact between sorbent and gas streams. The following reactions take place a in CaL system with a SEWGS unit for hydrogen production:

- carbonation and SEWGS reactor,

$$CO + H_2O + CaO \rightleftarrows CaCO_3 + H_2 \qquad \Delta H^0_{298} = -219\ kJ \cdot mol^{-1} \qquad (9)$$

- calcination reactor,

$$CaCO_3 \rightleftarrows CaO + CO_2 \qquad \Delta H^0_{298} = +183\ kJ \cdot mol^{-1} \qquad (10)$$

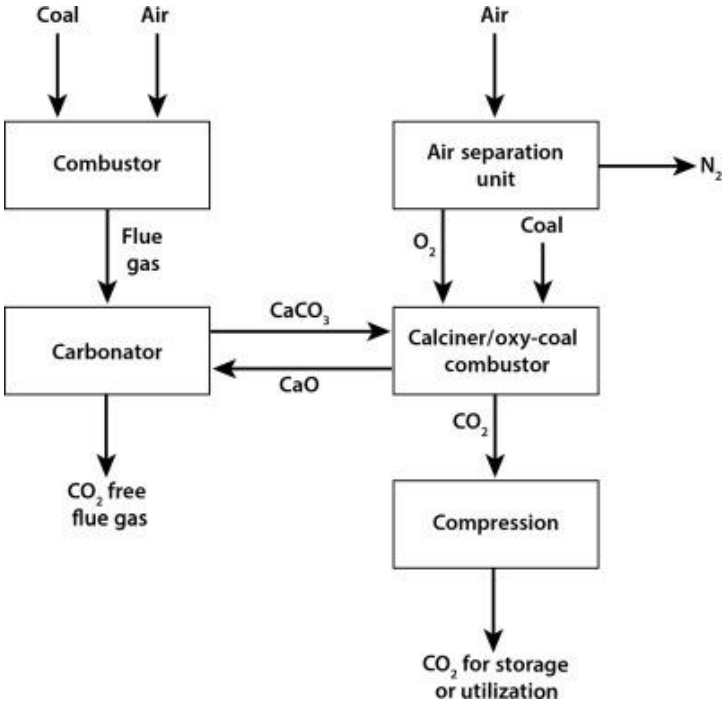

Figure 6. Schematic representation of a post-combustion CaL process [49]

The reasoning behind using oxy-combustion to supply energy for decomposition of $CaCO_3$ (Eq. (10)) is avoiding N_2 in the CO_2 stream. The ASU used to provide the oxygen adds energy penalties to the process, but some of the penalty can be offset by recovering energy from within the process using the high temperatures seen in the reactors (i.e., 650°C and 950°C in the carbonator and calciner, respectively) [50].

Power generation aside, CL technologies also show great potential in hydrogen production with intrinsic CO_2 removal.

The sorption-enhanced reforming (SER) process is adapting the conventional steam methane reforming (SMR) by adding a carbonation reaction to the reforming and water-gas shift reactions seen in the standard reforming process. In doing so, the H_2 purification section is simplified by combining hydrogen production and CO_2 removal into a single unit, the shift reactor and shift catalysts are eliminated, operating conditions are lowered leading to less expensive materials required, carbon deposition is reduced in the reformer, the overall energy requirement is reduced and a high purity CO_2 stream is produced, ready for storage or utilization in other applications [51].

Figure 7 shows the two interconnected CFB reactors utilized within SER. The reformer (i.e., carbonator) is responsible with H_2 production with intrinsic CO_2 separation (Eqs. (11) - (13)).

$$CH_4 + H_2O \rightleftarrows CO + 3H_2 \qquad \Delta H^0_{298} = +226\ kJ \cdot mol^{-1} \qquad (11)$$

$$CO + H_2O \rightleftarrows H_2 + CO_2 \qquad \Delta H^0_{298} = -41\ kJ \cdot mol^{-1} \qquad (12)$$

$$CO_2 + CaO \rightleftarrows CaCO_3 \qquad \Delta H^0_{298} = -183\ kJ \cdot mol^{-1} \qquad (13)$$

As can be seen from Eq. (11), the SMR reaction is endothermic, while the WGS (Eq. (12)) and carbonation (Eq. (13)) reactions are exothermic. The coupling of these three reactions within the reformer results in the carbonator operating at a borderline autothermal regime. The regenerator (i.e., calcinator) enables sorbent regeneration and produces a high concentration stream of CO_2 (Eq. (14)).

$$CaCO_3 \rightleftarrows CO_2 + CaO \qquad \Delta H^0_{298} = +183\ kJ \cdot mol^{-1} \qquad (14)$$

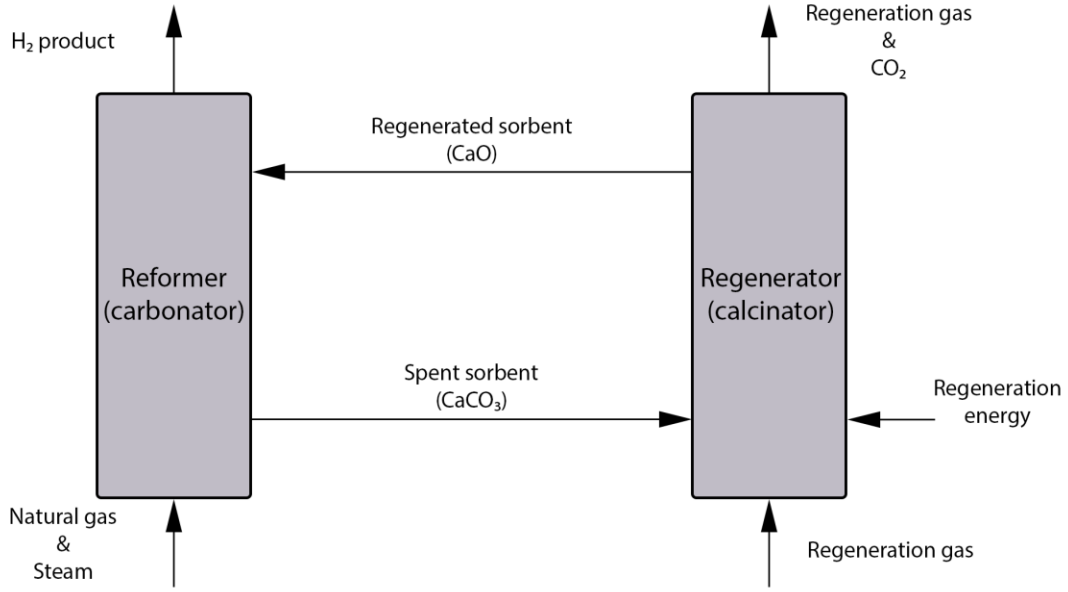

Figure 7. Schematic representation of the SER process with Ca-based sorbent

The CLH process [52], utilizing the three-reactor configuration shown in Figure 8, is based on the ability of Fe-based OCs to undergo oxidation with steam and generate hydrogen through the steam-iron reaction. The end product is very-high purity H_2 and intrinsic CO_2 capture without utilizing WGS reactors or PSA units for gas purification [52]. Eqs. (15) - (17) describe the reactions taking place inside the fuel reactor, the first step of the process, where the Fe-based OC reacts with fuel (i.e., methane) to result in a stream of CO_2 and H_2O, which can be condensed to obtain pure CO_2.

$$12Fe_2O_3 + CH_4 \rightleftarrows 8Fe_3O_4 + CO_2 + 2H_2O \qquad \Delta H^0_{298} = +230\ kJ \cdot mol^{-1} \qquad (15)$$

$$4Fe_3O_4 + CH_4 \rightleftarrows 12FeO + CO_2 + 2H_2O \qquad \Delta H^0_{298} = +420\ kJ \cdot mol^{-1} \qquad (16)$$

$$4FeO + CH_4 \rightleftarrows 4Fe + CO_2 + 2H_2O \qquad \Delta H^0_{298} = +278\ kJ \cdot mol^{-1} \qquad (17)$$

During the second step, hydrogen generation takes place in the steam reactor by adding excess steam to cause the partial oxidation of the Fe-based OC (Eqs. (18) and (19)).

$$Fe + H_2O \rightleftarrows FeO + H_2 \qquad \Delta H^0_{298} = -28\ kJ \cdot mol^{-1} \qquad (18)$$

$$3FeO + H_2O \rightleftarrows Fe_3O_4 + H_2 \qquad \Delta H^0_{298} = -63\ kJ \cdot mol^{-1} \qquad (19)$$

An air reactor is necessary, due to thermodynamic constraints, to realize the full oxidation of Fe_3O_4 to Fe_2O_3 using air (Eq. (20)) in the third step of the process. Additionally, the air reactor contributes as a thermal balance, resulting in an overall autothermal process.

$$2Fe_3O_4 + 1/2\ O_2 \rightleftarrows 3Fe_2O_3 \qquad \Delta H^0_{298} = -258\ kJ \cdot mol^{-1} \qquad (20)$$

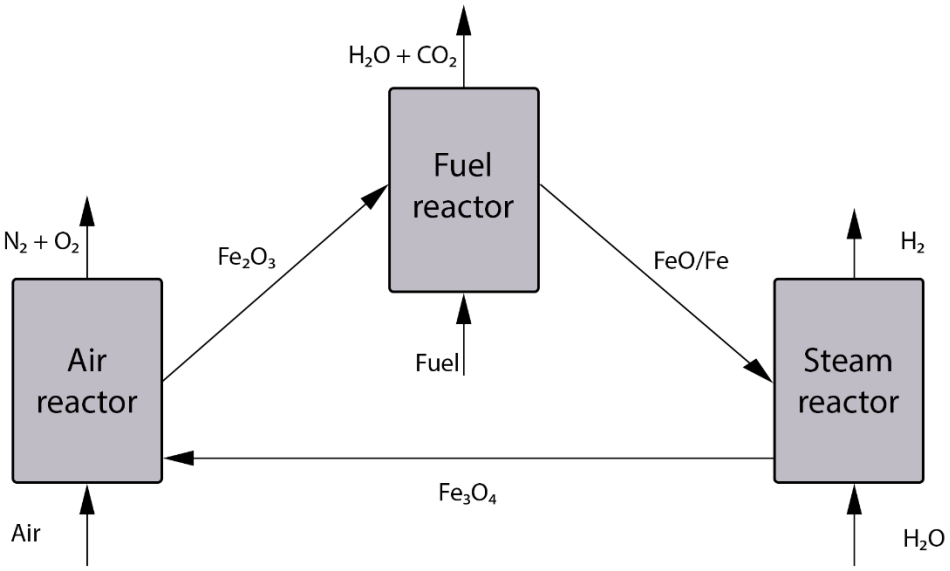

Figure 8. Schematic representation of the CLH process with Fe-based OC

Chapter 4 studies chemical looping technologies implemented at a small scale (i.e., reactor and OC particles), as well as various CL configurations applied to an industrial scale plant.

1.4. Goal and objectives

The scope of the thesis is to investigate different gas-solid processes applied to energy conversion systems with carbon capture. Carbon capture technologies combined with fossil fuel-based hydrogen production units could become a promising advancement towards reducing emissions of CO_2, as well as increasing energy efficiency and achieving higher output flexibility.

As of recent years, hydrogen has become one of the most compelling directions in global energy [53]. Hydrogen is a promising energy carrier, considered one of the most promising clean fuels to replace fossil fuels, due to the fact that no GHG emissions are produced when used in a fuel cell to generate electricity, only water vapor, as well as being sustainable, non-toxic and environmentally friendly [54]. Similarly to electricity, hydrogen production can be achieved by utilizing primary, both renewable (i.e., wind, solar, biomass, geothermal and flowing water) and non-renewable (i.e., oil, natural gas, coal and nuclear sources), or secondary sources of energy [55]. Moreover, hydrogen can be used directly in different industrial processes or stored as fuel, making power-to-gas extremely attractive during periods of excess electricity generation [56].

Hydrogen is expected to add significant contributions towards decarbonisation of high-temperature industrial heat, by replacing the large consumption of fossil fuel following modifications of the burner systems to deal with the specific combustion characteristics of hydrogen.

Up until 2021, low-emissions hydrogen fuel has seen limited applications, but it has considerable promise to replace hydrocarbon-based fuels in heavy and long-distance road transport vehicles (i.e., buses, trucks) and ships. Finally, hydrogen can provide flexibility to power systems by becoming a storage medium for electricity generation [57].

Most of the hydrogen produced in 2020 (see Figure 9 for sources), 70 Mt of pure hydrogen and 120 Mt total hydrogen (counting syngas), was utilised in oil refineries and the chemical industry. The share of hydrogen currently being produced in 2020 from coal, through gasification, and natural gas, through SMR, is 98%, both processes emitting considerable amounts of CO_2 if not captured [58]. Aside from production of hydrogen from fossil fuels with CCS, the other low-carbon hydrogen production route is through water electrolysis powered by renewables, currently accounting for 0.3%.

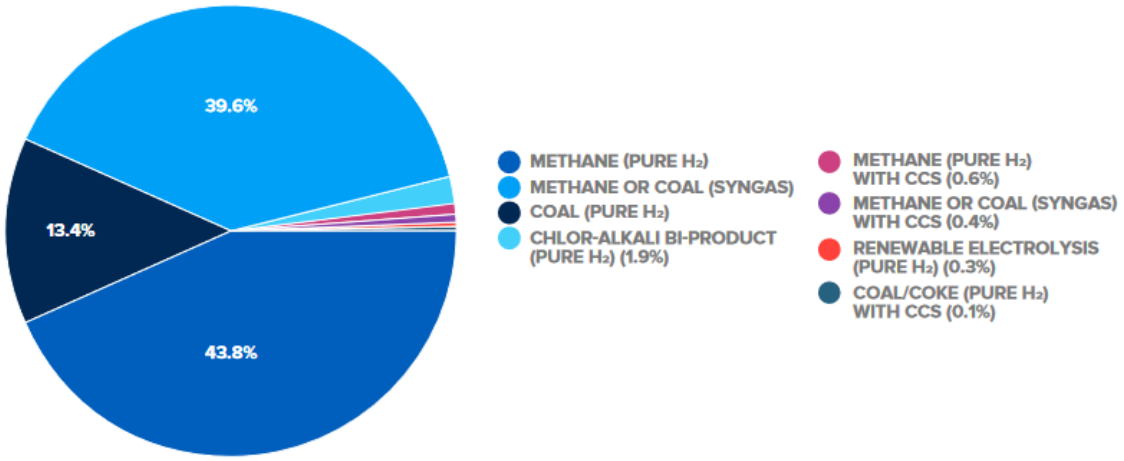

Figure 9. Shares of global hydrogen production from various sources [13]

Currently, most of the hydrogen production is through unabated coal and gas, emitting around 830 Mtpa CO_2, as reported by the IEA in 2019 [57]. Around 0.7% of total hydrogen generation is from renewable sources via electrolysis and CCS-equipped fossil fuel plants [59]. Consequently, achieving the goal of net-zero emissions by 2050 will require considerable efforts in retrofitting carbon capture on existing units, as well as deploying new CCS plants.

The alternatives for hydrogen production through coal gasification and SMR with CCS present a significantly lower cost than water splitting (i.e., electrolysis) from renewables. IRENA [54] reported that hydrogen generation using renewables should become cost-competitive with production through CCS-adapted coal gasification and SMR by 2050.

SMR is considered a mature technology and is the main method through which hydrogen is produced, by reacting methane and steam at high temperatures. Subsequently, a shift reactor enables the conversion of the resulted carbon monoxide into more hydrogen by reacting with steam through WGS.

Moreover, combining the WGS reaction with the adsorption process of CO_2 leads to a pre-combustion technology known as SEWGS. SEWGS is currently a developing technology with very high potential in mitigation of industrial CO_2 emissions, as evidenced by Manzolini et al. [60] who reported SEWGS outperforming amine scrubbing, considered the benchmark of carbon capture technology, when integrated into an iron and steel plant for power generation.

Another promising solution towards achieving carbon neutrality until 2050 is CLC, through which the continued usage of fossil fuels is possible by generating power with low GHG emissions. CLC, still being developed, is promising for both power plants, as well as industrial operations, as it enables fossil fuel combustion with inherent CO_2 capture, leading to a direct reduction of the energy penalties typically imposed by the integration of carbon capture seen in competing technologies [61].

To this end, the three evaluated processes in this work are water-gas shift, sorption-enhanced water-gas shift and chemical and calcium looping technologies.

Following an in-depth literature review to comprehend the status of research of the aforementioned processes, thorough investigation was performed by means of process flow diagram design, modelling and simulation, as well as technical and thermal integration aspects, with the purpose of process intensification, process performance enhancement or extracting useful data to be used in process scale-up.

2. Assessment methodology

2.1. Gas-solid reactor modelling and simulation

The software tools used in this work for the development of complex mathematical models of reactors for energy conversion were MATLAB/Simulink and COMSOL Multiphysics.

2.1.1. MATLAB/Simulink

MATLAB and Simulink are commonly used together to combine textual and graphical programming in designing the desired system, enabling the incorporation of algorithms written in MATLAB into models and the export of the simulation results back to MATLAB for further analysis. The programming code can be written in MATLAB and added into a Simulink block to be used in the simulation environment alongside the basic blocks available in the library [62].

In this work, the S-function block provided by Simulink was used simulate dynamic models built using MATLAB to define the S-function block characteristics and differential equations. S-functions (i.e., system functions) represent an advanced method through which the Simulink environment and its capabilities can be expanded. Specifically, an S-function is the description through programming language of the Simulink block written in MATLAB. The way S-functions work is by defining how the block behaves during different steps of the simulation (i.e, initialization, updates, derivatives, outputs and termination). Methods are invoked by the simulation engine to complete specific tasks during every simulation step. Fundamental understanding of the mathematical relationships seen between block inputs, outputs and states is required, as well as the way Simulink simulates models (i.e., the stages of simulation) [63].

The Simulink block (as seen in Figure 10) is comprised of sets of inputs, states, parameters and outputs, represented mathematically in Eqs. (21) - (23). The outputs are functions of inputs, parameters, states and simulation time [64].

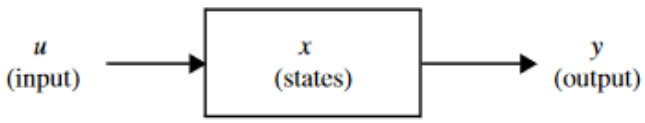

Figure 10. Basic representation of a Simulink block

$$y = f_0(t, x, u) \qquad (Output) \qquad (21)$$

$$x_c = f_d(t, x, u) \qquad (Derivative) \qquad (22)$$

$$x_{d_{k+1}} = f_u(t, x, u) \qquad (Update) \qquad (23)$$

where x is the sum of x_c and x_d.

2.1.2. COMSOL Multiphysics

COMSOL Multiphysics is a powerful simulation environment used to build and solve models in all fields of engineering and scientific research. Numerous real-world applications require simultaneous couplings of physics, which can be represented in a system of partial differential equations (PDEs). PDEs are the class of equations commonly used in science and engineering to describe all phenomena present in the physical world and represent the foundatiosn for complex mathematical modelling. For most-real world problems, there are no closed-form solutions to PDEs. Therefore, it is necessary to discretize the continuous PDEs with numerical model equations and use numerical solving methods to approximate the solution at discrete points in the domain. COMSOL uses the finite element method (FEM) to compute the approximations [65].

Depending on the problem in question, a direct or iterative solver will generally be used to efficiently solve the system of equations while maintaining a balance between performance and robustness. Direct solvers are useful for smaller problems with less degrees of freedom, while iterative solvers are more efficient for larger models.

COMSOL enables a smooth transition from regular single-physics models and easily extends them into multi-physics models capable of simultaneously solving multiple coupled physics phenomena with either stationary or transient and linear or nonlinear study types.

During model solving, the software assembles and solves the underlying set of equations representing the entire model using a variety of advanced numerical tools that account for error control and adaptive mesh refinement, if enabled. After the model converges and simulation results are available, COMSOL provides the postprocessing and visualization tools necessary to evaluate the solution and present the results in a clear way [65].

A mesh convergence study confirms that the FEM model has converged to an accurate solution. The process involves decreasing the element size and evaluating the effects on the precision of the solution. A formal method used to estimate mesh convergence consists of graphically representing a critical result

variable as a function of mesh density. After at least three simulation runs, the resulting curve can be used to establish if mesh convergence was achieved or if further mesh refinement is required.

The mesh refinement process necessary to establish mesh convergence is the final step in FEM modelling. There are many techniques for mesh refinement being commonly used depending on the particular problem, physical geometry and experience of the FEM user.

The current work used COMSOL Multiphysics to develop several complex CFD models in one, two and three spatial dimensions, accounting for mass, heat and momentum transfer, to be simulated in transient state with the purpose of investigating various gas-solid systems at different orders of dimensions such as macro- and micro-scale.

2.2. Process flow modelling

2.2.1. CHEMCAD

The process simulation software used in this work for design, development, analysis and optimization of the proposed processes was ChemCAD, a commercial chemical process simulator developed by Chemstations. The advantage of using ChemCAD as a chemical process simulation environment is the access to large libraries of thermodynamic data and common unit operations, allowing the seamless simulation of chemical processes seen in a wide variety of industries, ranging from oil and gas production and refining to gas processing, pharmaceuticals, biofuels and process equipment manufacturing. Additionally, the software exhibits adaptability and flexibility by allowing customization of chemicals, thermodynamics, unit operations, calculations and reporting. ChemCAD is capable of modelling all types of processes, such as batch, semi-batch and continuous, and can run simulations of steady-state and dynamic systems [66].

The current work utilized ChemCAD to design flowsheets for complex gas-solid systems and run steady-state simulations in order to acquire mass and energy balances to be used in techno-economic assessments.

2.3. Technical evaluation

Technical analysis is mandatory to evaluate the performance and potential of a process. A means of performance measurement are key performance indicators (KPIs). Since KPIs are linked to target values, they enable a direct comparison of similar processes in regards to performance. Mass and energy balances are obtained from process flow modelling software (i.e., CHEMCAD) and used to calculate KPIs. The

following KPIs are used to establish performance estimations in energy conversion systems with and without carbon capture:

- Gross and net power efficiencies are calculated by dividing the gross and net output power, respectively, by the input power, thus, for gross power efficiency,

$$\eta_{gross} = \frac{P_{gross}}{\dot{m}_f \cdot LHV_f} \cdot 100\% \tag{24}$$

where P_{gross} is gross electric power output, $\dot{m}_f$ is mass flow rate of the fuel and LHV_f is low heating value of the fuel, and for net power efficiency,

$$\eta_{net} = \frac{P_{net}}{\dot{m}_f \cdot LHV_f} \cdot 100\% \tag{25}$$

where P_{net} is net electric power output;

- Carbon capture rate (CCR) is calculated as the ratio of molar flow of captured CO_2 to carbon molar flow from the feedstock (Eq. (26)),

$$CCR = \frac{F_{CO_2,captured}}{F_{feedstock\ carbon}} \cdot 100\% \tag{26}$$

- CO_2 specific emission rate is calculated by considering emitted CO_2 mass flow for each MW of net generated power (Eq. (27)),

$$CO_2\ specific\ emission\ rate = \frac{\dot{m}_{CO_2,emitted}}{P_{net}} \tag{27}$$

where $\dot{m}_{CO_2,emitted}$ is mass flow rate of emissions of CO_2;

- Specific primary energy consumption for CO_2 avoided (SPECCA) is calculated by considering net energy efficiencies and CO_2 emissions for the concepts with and without CCS (Eq. (28)),

$$SPECCA = \frac{3600\left(\frac{1}{\eta_{net}} - \frac{1}{\eta_{net,ref}}\right)}{E_{CO_2,ref} - E_{CO_2}} \tag{28}$$

where $\eta_{net,ref}$ is net electrical efficiency of the reference system without CCS, $E_{CO_2,ref}$ is the specific emission rate of CO_2 of the reference system without CCS and $E_{CO_2,ref}$ is the specific CO_2 emission rate of the investigated system.

Some designs consider production of energy vectors alongside electrical energy, for instance hydrogen. Estimation of hydrogen production efficiency can be done similarly to the electrical energy efficiency estimation, shown in Eq. (24), by replacing electric power output with the output of hydrogen. Hydrogen

production efficiency, further used to estimate co-generation-related KPIs, was calculated using Eq. (29). For designs in which both electricity and hydrogen are being generated, a cumulative energy efficiency can be determined as the sum of efficiencies of the two energy outputs (Eq. (30)).

$$\eta_{H_2} = \frac{Hydrogen\ thermal\ output\ [MW_{th}]}{Thermal\ energy\ of\ used\ fuel\ (coal)\ [MW_{th}]} \cdot 100\% \quad (29)$$

$$\eta_{cumulative} = \eta_{net} + \eta_{H_2} \quad (30)$$

Ancillary power consumption (APC) is a another useful KPI, as part of the energy generated in the power plant is consumed by different auxiliaries (i.e., operation of various processes and equipment) and is responsible for adding an efficiency penalty to CCS equipped power plants, mainly due to the energy-intensive processes within the carbon capture system (i.e., primarily CO_2 compression). Thus, a reduction in APC is desired in order to improve overall system efficiency and reduce power plant costs. APC is related to net power output and gross power output by Eq. (31):

$$P_{net} = P_{gross} - APC \quad (31)$$

2.4. Thermal integration

Heat integration is paramount in enhancing energy efficiency and decreasing operating costs in energy related applications, such as energy conversion systems with carbon capture. The focus of heat integration is on reduction of hot and cold utilities, due to the fact that thermal energy is a significant contributor to process costs. Therefore, when feasible, application of waste heat recovery technologies will always prove an attractive alternative to consuming additional energy for heating duties [67].

A well-established tool used in process design to attain minimum utility requirements is pinch analysis (PA). Opportunities for energy recovery can be identified by investigating individual process units or the entire system. The systematic methodology is based on the process flow diagram, as well as the material and heat balances of the process [68]. Simply put, heat exchangers are inserted to couple streams in need of heating to streams in need of cooling. Identifying which process streams are in need of heating or cooling is achieved with composite curves (CC).

Initially, the enthalpy flux change is calculated using Eq. (32) [69], based on supply and target temperatures of streams within the process (i.e., stream temperatures before and after energy integration, respectively).

$$\Delta H = \dot{m} \cdot Cp \cdot (T_{in} - T_{out}) \quad (32)$$

where $\dot{m}$ is mass flow rate of the stream, *Cp* is specific heat capacity, T_{in} is the stream inlet temperature and T_{out} is the stream target outlet temperature.

Moreover, alongside sensible heat changes, a significant contribution to enthalpy change stems from phase changes (i.e., condensation and evaporation), which can be calculated with Eq. (33):

$$\Delta H = \dot{m} \cdot \lambda \tag{33}$$

where $\dot{m}$ and λ is mass flow rate and latent heat, respectively, for the stream undergoing condensation or evaporation.

The CCs (i.e., temperature-enthalpy diagrams) can then be constructed separately for the hot and cold streams. The horizontal segments seen in the hot and cold composite curves represent the latent heat of condensation and vaporization, respectively.

3. Investigation of WGS and SEWGS processes

3.1. Evaluation of SEWGS with CFD modelling

The scope of this chapter is the investigation of SEWGS, more specifically the adsorption step of the process. The goal of the research was to achieve a productivity increase for SEWGS using 3D-printed structured bed reactors, as opposed to the conventional packed bed reactors, by taking advantage of the reduced mass transfer limitations and pressure drops provided by structuring.

Monoliths are the starting point for this work, as they provide many benefits as explained above. However, the novelty of this work lies in the fact that 3D-printing allows for producing more complex structures that cannot be obtained by traditional manufacturing methods once the structure-productivity relations are well understood and can be modelled.

This chapter presents numerical modelling and simulation work backed by experimental and numerical validation methods with the goal of investigating packed bed and monolith reactors used in SEWGS in regards to performance and provide insight into the enhanced mass transfer efficiency provided by the structured bed reactor. To this end, several CFD models were developed using COMSOL Multiphysics.

The following CFD models were developed to study a monolith reactor with rectangular channels:

- 1D fixed bed reactor model was initially required for indirect model validation of the monolith reactor model with straight channels, as experimental data were not available to enable model validation;
- 2D structured bed reactor model with straight channels;
- 2D structured bed reactor models with different channel configurations to evaluate geometry related mass transfer effects.

To properly assess the efficiency of mass transfer for each specific geometry, the relative CO_2 mole fraction was plotted versus relative time (Figure 11). The conic geometry with a smaller inlet showed the steepest breakthrough curve, indicating that the bed was being utilized more efficiently. One explanation was the incoming cold flux decreasing the temperature where adsorption had already taken place, increasing the capacity further. In the case of the cone with a smaller inlet, the portion near the channel entrance had the most amount of adsorbent mass out of all studied geometries, meaning the effect of heat transfer over the adsorption capacity was the most significant.

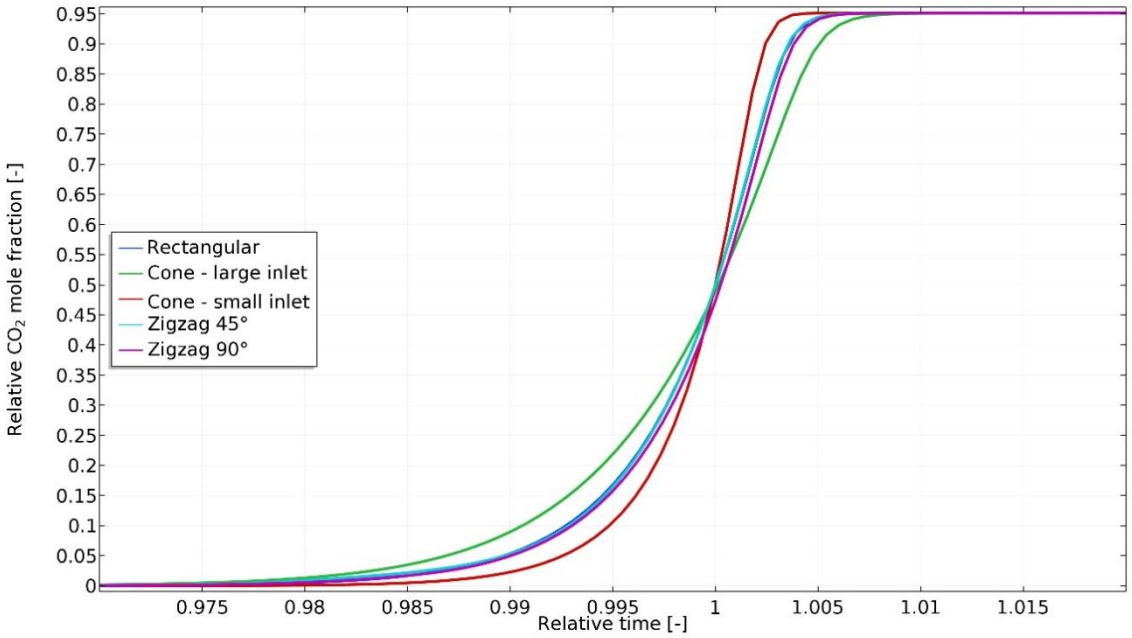

Figure 11. CO_2 mole fraction at the reactor outlet relative to the mole fraction of the feed gas vs. relative time calculated by the CFD monolith reactor models for different geometries

By analysing simulation results of the developed 2D models for adsorption in channels of different geometries with respect to mass transfer resistance, it can be concluded:

- The presence of WGS led to faster breakthrough due to formation of CO_2, however, the breakthrough curves predicted completely overlapped, meaning that mass transfer can be analysed using models without taking WGS into account;
- Although comparison between geometries considered the same mass of adsorbent, slightly different loading values and breakthrough times were predicted for the various geometries, mainly due to the differences in heat transfer induced by each respective geometry;
- Judging by the profiles of the breakthrough curves and mass transfer zones, the cone shaped geometry with a smaller inlet section showed the most efficient utilization of the adsorbent, highest transfer rates and least mass transfer resistance, followed by the rectangle and zigzag geometries;
- There was better diffusion of the CO_2 and H_2O induced by the local flow due to the more complex path and increased mixing of the gas in the case of the layouts with zigzag setups, increasing the concentration of these components at the gas-solid interface and also enhancing the adsorption process. An interesting approach might be having a larger adsorbent mass near the inlet, while using a zigzag setup for the rest of the geometry;
- Pressure drop was lower for the structured bed models when compared to estimated packed bed pressure drop;

- The ratio between the channel dimensions and the sorbent mass was significant and could be an important limitation for the adsorption capacity in the monolith reactor.

In order to evaluate monolith channel shape (i.e., circular, square and hexagonal), as well as investigate which spatial dimensions (i.e., 2D, 3D) yield more accurate results in terms of model predicted breakthrough times, the following CFD models were developed:

- 2D vs. 3D comparison of single channel models for geometry assessment.

CO_2 breakthrough curves predicted by all 2D and 3D models can be seen in Figure 12. Since the mass of adsorbent material was the same for the 3D models, the breakthrough times should be similar. The geometrical differences between 2D models were extremely small, as the 2D geometries were represented by a cross-section of the 3D geometries; thus, the breakthrough times should also be similar.

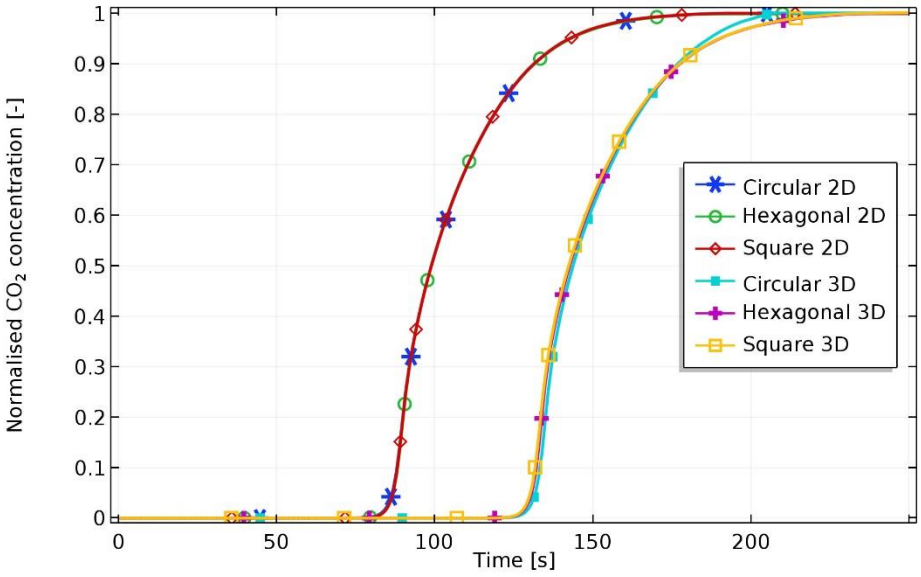

Figure 12. CO_2 model predicted breakthrough curves

The results show that the differences between the full 3D models and the simplified 2D models are significant in term of breakthrough time, but also in the case of necessary computational resources. For the 3D models the predicted breakthrough time is about 140 s and for the simplified geometry models is about 100 s due to the fact that the volume/mass of the adsorbent monolith in the simplified 2D geometry could not be well defined and did not consider the true shape of the structure, leading to different characteristic values of the considered phenomena (flow velocities, pressure drops, dispersion and diffusion rates). The other explanation behind the differences in the predicted velocity profiles stems from the missing velocity vector in the third coordinate axis for 2D models.

A transition from 2D to 3D with the purpose of enhanced precision, as well as the possibility of direct validation using bench-scale 3D-printed structures, led to the development of the following CFD models:

- 3D structured bed bench-scale reactor model with straight hexagonal channels, validated using breakthrough measurements on 3D-printed structures;
- 3D structured bed reactor models with different zigzag channel configurations to investigate geometry related mass transfer effects;
- 1D multiscale fixed bed model, validated using experimental data;
- 3D structured bed lab-scale reactor model with straight hexagonal channels to enable a comparison of mass transfer rate with the validated packed bed configuration.

Figure 13 compares the normalized breakthrough curves predicted by the straight channel and zigzag channel models at three different flow rates. The zigzag configuration showed a sharper breakthrough curve for all considered flow rates, with the effect on mass transfer efficiency increasing at higher flow rates, which is expected since a higher degree of mixing is seen at higher Reynolds values.

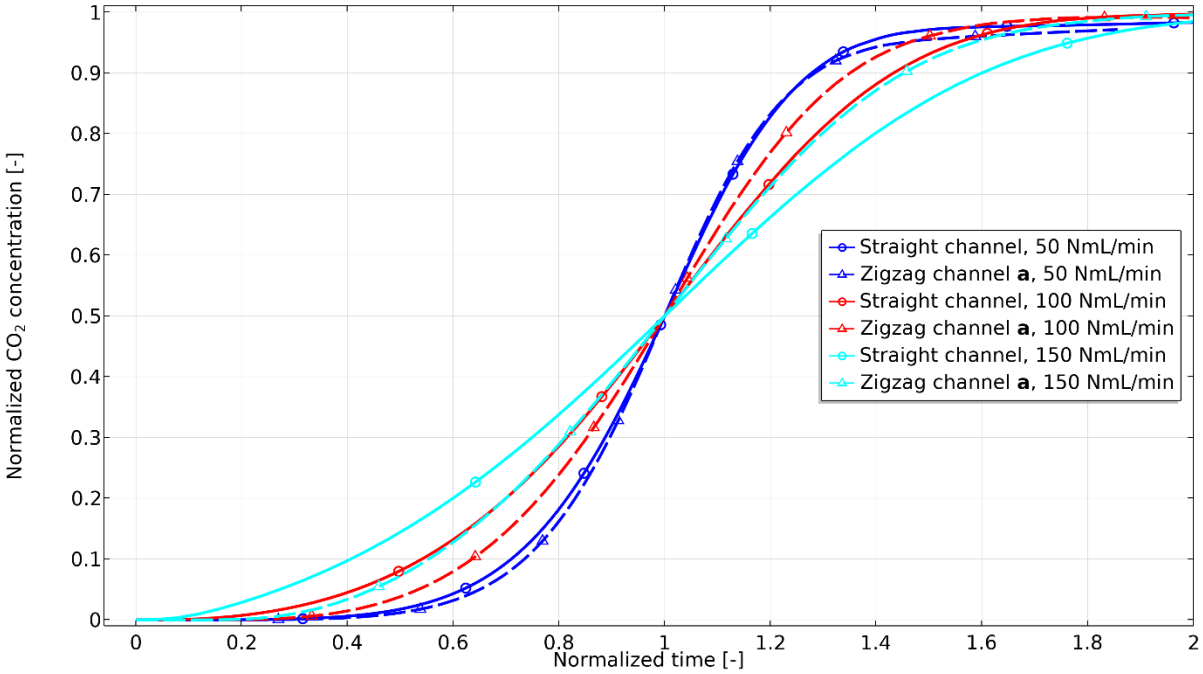

Figure 13. Normalized CO_2 breakthrough curves for zigzag channel (a) vs. straight channel predicted by the bench-scale monolith model at different flow rates and atmospheric pressure

Moreover, the three different zigzag channel configurations were evaluated in terms of bed utilization. All zigzag channel configurations exhibited sharper mass transfer rates when compared to the straight channel structured bed reactor. Following a scale-up of the bench-scale model, a comparison between packed bed and monolith reactors took place with focus on mass transfer efficiency.

Figure 14 shows the experimental and predicted breakthrough curves for the packed bed configuration, as well as the predicted breakthrough curve by the monolith model for the flow rate of 25 $NL \cdot min^{-1}$. CO_2 concentration was plotted as a function of time. For the packed bed data sets, the profiles of the curves were

very similar, with breakthrough starting at around the same point in both cases. A breakthrough point was considered at a relative concentration (i.e., fraction of outlet concentration over inflow concentration) of 0.5 and the times predicted by the packed bed and monolith models were in agreement with the experimental time (seen in the annotation in Figure 14), which was expected as the sorbent mass was identical for all cases. It can be noticed that mass transfer was slower for the packed bed configuration, since the breakthrough curves were not as sharp as the monolith model predicted breakthrough curve. The sorbent was entirely utilized at 28.4 min, as predicted by the monolith model, versus 35 min, predicted packed bed reactor model, indicating a performance increase of 23.23% when considering SEWGS using a structured bed configuration. Furthermore, the mass transfer zone calculated by the monolith model was shorter when compared to the mass transfer zone corresponding to the packed bed model, indicating a more efficient utilization of the bed.

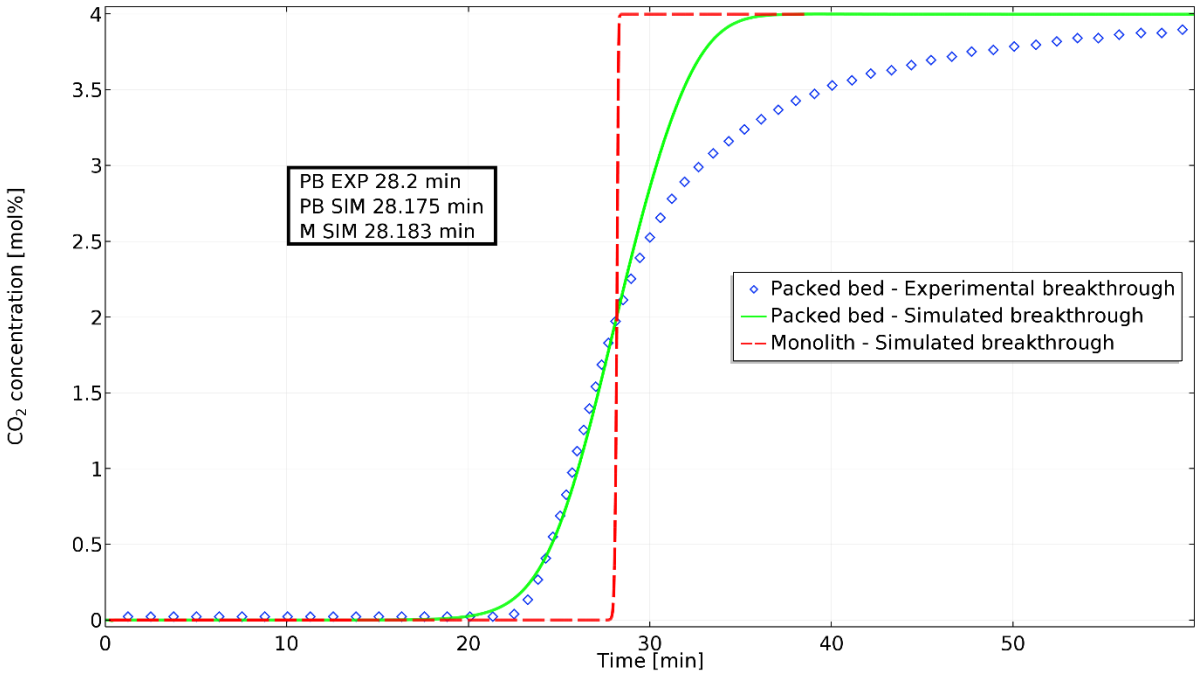

Figure 14. Experimental (blue diamonds) and simulated (green) CO_2 breakthrough curves for packed bed reactor case and simulated (red) CO_2 breakthrough curve for monolith reactor case

3.2. Various WGS configurations for IGCC power plant with CO_2 capture

This chapter evaluates the WGS (Eq. (3)) conversion of syngas through various configurations [70,71]. The assessments are geared towards the evaluation of process configurations on key plant performance indicators (e.g., overall energy efficiency, ancillary energy consumptions, carbon capture rate, specific CO_2 emissions) of various WGS conceptual designs. The assessed WGS process options are:

- Conventional catalytic conversion using 2-3 reactors in series either in clean shift conditions (with applications in natural gas reforming technologies) or sour shift conditions (with applications in coal gasification);
- FeL cycle using three interconnected CFB reactors;
- CaL cycle using two interconnected CFB reactors where calcium-based sorbent is used to move the WGS equilibrium to the right according to the reactions presented in Eqs. (9) and (10) are occurring.

Table 1 presents the main performance indicators of evaluated IGCC with carbon capture designs operated in power generation only.

Table 1. Overall plant performance indicators – power generation only

Main Plant Data	**Units**	**Case 1**	**Case 2**	**Case 3**
Coal flow rate (a.r.)	$t \cdot h^{-1}$	165.00	162.00	225.00
Coal LHV (a.r.)	$MJ \cdot kg^{-1}$		25.353	
Coal thermal energy (A)	MW_{th}	1162.00	1140.88	1584.56
Gas turbine output (M701G2)	MW_e	334.00	334.00	334.00
Steam turbine output	MW_e	201.25	200.00	411.25
Expander power output	MW_e	1.01	1.25	1.40
Gross electric power output (B)	MW_e	536.26	535.25	746.65
Ancillary consumption (C)	MW_e	110.67	95.75	152.82
Net power output (D = B - C)	MW_e	425.59	439.50	593.83
Gross efficiency (B / A × 100)	%	46.15	46.91	47.12
Net efficiency (D / A × 100)	%	36.62	38.52	37.47
Carbon capture rate	%	90.00	99.00	96.00
CO_2 specific emissions	$kg \cdot MWh_e^{-1}$	83.24	4.10	33.50

The high temperature looping cases (FeL and CaL) have superior overall net efficiency (by about 0.9 points - 1.9 points) and carbon capture rate (90% vs. 96% - 99%) than conventional WGS catalytic conversion coupled with reactive gas-liquid absorption for CO_2 capture. These results show the good potential of chemical looping technology, capable of simultaneously converting the syngas energy in a decarbonized energy carrier, hydrogen, and capturing carbon from syngas, to replace conventional technologies in the future, such as catalytic WGS conversion and gas-liquid absorption.

Ancillary energy consumption of carbon capture unit is a factor with paramount importance in any carbon capture, utilization and storage (CCUS) design. In this respect, the reactive gas-liquid systems have a clear disadvantage, as exemplified here by MDEA-based system, due to the significant heat duty required to regenerate the solvent of about 3 $MJ \cdot kg^{-1}$ CO_2. To evaluate the ancillary energy consumption for CO_2 capture in a holistic manner, SPECCA was calculated using Eq. (28) [72].

For an IGCC power plant benchmark case without capture, key literature references such as International Energy Agency Greenhouse Gas R&D Programme (IEAGHG) and National Energy Technology Laboratory (NETL) reports were used [73,74]. The SPECCA values calculated for the investigated concepts (Cases 1-3) are 2.75 $MJ \cdot kg^{-1}$, 1.88 $MJ \cdot kg^{-1}$ and 2.36 $MJ \cdot kg^{-1}$, respectively. As also showed by SPECCA indicator, the reactive gas-solid systems (FeL and CaL cycles) have lower energy consumptions for CO_2 capture than the reactive gas-liquid system.

An important feature of gasification plants coupled with pre-combustion CO_2 capture, exhibited here by all investigated concepts, is the ability of hydrogen and power co-generation [75–77]. These plants can generate, according to the instant power demand from the grid, either only electricity at peak times, hydrogen and power during transient times or only hydrogen for energy storage, when power generation is low. This operational flexibility can be obtained by a simple operational procedure of gradually turning down the gas turbine to displace a hydrogen stream for purification, followed by energy storage. To illustrate the ability of hydrogen and power co-generation, Table 2 presents the variation of performance indicators with hydrogen produced in the range 0 MW_{th} - 200 MW_{th} for Case 2.

Table 2. Overall plant performance indicators – hydrogen and power co-generation

Main Plant Data	**Units**	**Power**	**Hydrogen and power**	
Coal flow rate (a.r.)	$t \cdot h^{-1}$		162.00	
Coal LHV (a.r.)	$MJ \cdot kg^{-1}$		25.353	
Coal thermal energy (A)	MW_{th}		1140.88	
Gas turbine output (M701G2)	MW_e	334.00	294.28	253.10
Steam turbine output	MW_e	200.00	181.01	162.24
Expander power output	MW_e	1.25	1.20	1.15
Gross electric power output (B)	MW_e	535.25	476.49	416.49
Hydrogen output (C)	MW_{th}	0.00	100.00	200.00
Ancillary consumption (D)	MW_e	95.75	94.33	92.84

Net power output (E = B - D)	MW_e	439.50	382.16	323.65
Net efficiency (E / A × 100)	%	38.52	33.49	28.36
Hydrogen efficiency (C / A × 100)	%	0.00	8.76	17.53
Cumulative energy efficiency	%	38.52	42.25	45.89
Carbon capture rate	%	99.00	99.00	99.00
CO_2 specific emissions	$kg \cdot MWh^{-1}$	4.10	3.73	3.44

As can be noticed, the hydrogen and power co-generation have a positive influence on cumulative plant energy efficiency, the indicator increasing with the hydrogen output by about 3.7 net cumulative efficiency points for each 100 MW_{th} of hydrogen produced. Other positive changes can be observed such as slight decrease of ancillary energy consumption, by about 1.5 MW_e per each 100 MW_{th} hydrogen, and specific CO_2 emissions, when considering the total plant energy produced. In addition to the technical performance indicators, the economic indicators, e.g., specific capital investments, operational and maintenance cost, CO_2 avoidance costs, are also improving with hydrogen coproduction [77].

As the results show, the looping cycles proved significant advantages compared to conventional design, i.e., higher overall plant energy efficiency by about 0.9 net efficiency points - 1.9 net efficiency points, higher carbon capture rate of 96% - 99% vs. 90% and lower SPECCA values by about 0.4 $MJ \cdot kg^{-1}$ - 0.9 $MJ \cdot kg^{-1}$.

The hydrogen and power co-generation based on IGCC design with carbon capture had also significant operational advantages: better plant flexibility (cycling), higher overall (cumulative) efficiency, with 3.7 net energy efficiency points per each 100 MW_{th} hydrogen, and better techno-economic indicators.

4. Investigation of chemical looping technologies

Complex mathematical models were developed to investigate CLC systems in a fixed bed configuration, as opposed to the conventionally seen fluidized bed arrangement. The OC considered for all models was ilmenite. Dynamic models, accounting for mass and heat transport, were developed in MATLAB/Simulink to simulate all three alternating steps in a stationary CLC process (i.e., reduction, oxidation, purge) considering methane and syngas as fuel.

In addition, CFD modelling was used to simulate the reduction and oxidation steps with syngas in a stationary CLC process by developing a 1D multiscale fixed bed reactor model in COMSOL Multiphysics, accounting for mass, heat and momentum transport. A good fit between experimental and simulated data was seen, as evidenced by the reported correlation coefficients. Subsequently, a 3D single particle model was developed to provide additional understanding regarding influence of mass and heat transfer processes on reduction rate of an iron-based oxygen carrier with syngas.

Finally, the chapter evaluates essential mass and energy integration aspects of chemical and calcium looping cycles used for pre-combustion CO_2 capture in an IGCC power plant. The evaluated mass and energy integration elements were analysed as essential methods to increase the global energy conversion yield. The modelling and simulation work was performed using CHEMCAD software.

4.1. Dynamic modelling of CLC of methane and syngas in packed bed reactors

Conventional CLC systems are designed using fluidized bed reactors, where the OC is transported in a loop between fuel and air reactors. Chapter 4.1 presents dynamic mathematical models developed in MATLAB/Simulink to evaluate a fixed bed configuration for a CLC system with stationary ilmenite OC. The two models take into account all CLC steps (i.e., oxidation, reduction, purge) and evaluate reduction with methane and syngas, respectively.

A graphical representation of the dynamic CLC reactor considering combustion of methane is shown in Figure 15. The OC considered was activated ilmenite, an iron/titan oxide. Furthermore, this work assumed only iron-based OC, with the simplified oxidation and reduction reactions. The ferric component was Fe_2O_3, while the ferrous one was represented by FeO. Initially, methane gas enters the fuel reactor, filled with the ilmenite particles, where OC reduction takes place. After the oxygen from the carrier is exhausted, the inflow of methane is stopped and a purge step takes place with a CO_2 stream to remove the unreacted methane. Subsequently, a stream of air enters the air reactor during the regeneration step, in which the oxidation reaction occurs. Finally, after the iron-based OC is regenerated, another purge step

with CO_2 is required to clear the unreacted oxygen and provide a better use of the heat produced during oxidation. The OC undergoes a conversion cycle until solid inactivity is noticed.

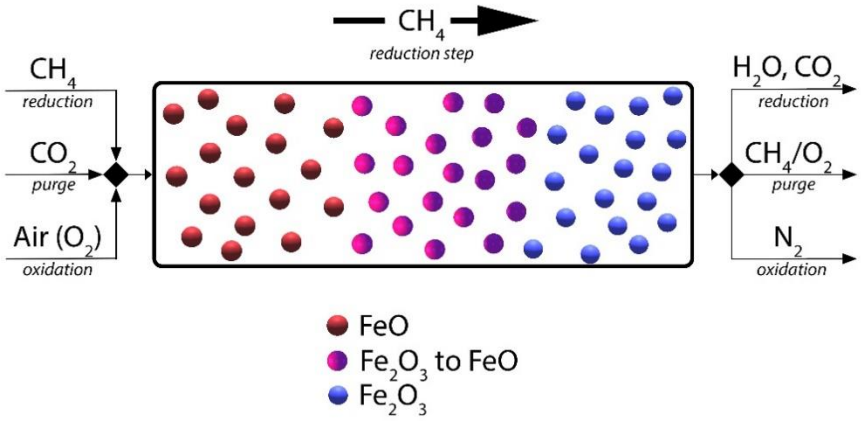

Figure 15. During the reduction step CH_4 reacts with Fe_2O_3 leaving behind inactive FeO. The CLC reactor cycles through four steps: reduction, purge, oxidation and purge once more, before beginning another cycle

The dynamic nature of the CLC reactor with alternating operation of the fuel and air reactors is highlighted in Figure 16, showing operation of three full cycles.

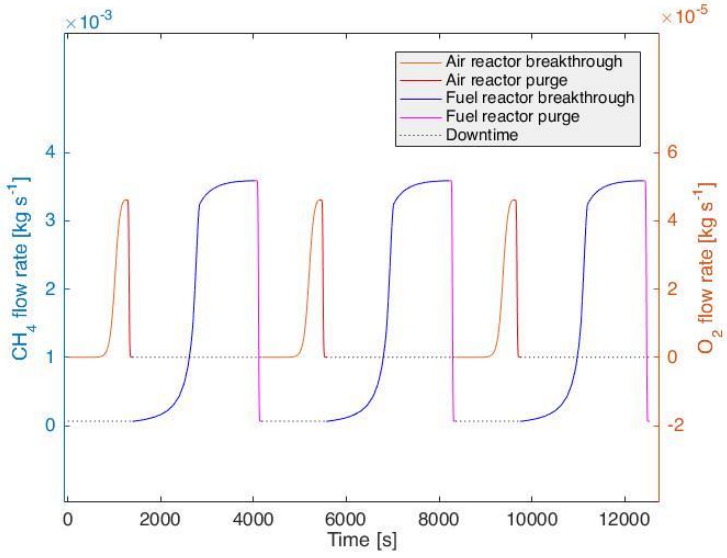

Figure 16. CH_4 and O_2 flow rates as functions of time during three full cycles for the CLC reactor

Both models were validated using literature data, as model predictions were in accordance with published experimental measurements.

Based on the results predicted by the model simulating CLC of methane, variation of the oxygen flow rate had a significant impact on the total time required to reach complete conversion of the OC. A flow rate increase of the air stream by 20% indicated the system reached a stationary state in less time by 200 s, while the decrease by 20% in air flow rate revealed a longer time needed to reach steady state by 300 s.

Model scale-up is possible and relatively straightforward, as the model equations remain the same. Switching the model parameters enables an investigation into the system's dynamic behaviour and optimal operating conditions at an industrial level.

4.2. Syngas-based CLC in packed bed reactors with CFD modelling

This chapter presents the investigation by means of CFD modelling of CLC of syngas with ilmenite. A multiscale model was developed in COMSOL Multiphysics to describe the behaviour of the reduction and oxidation reactions in a fixed bed system. Moreover, a 3D single particle CFD model was developed to simulate the reduction phase and analyse the intraparticle phenomena occurring within the ilmenite granule, with particular emphasis on heat transfer effects.

The research is based on numerical modelling and simulation work supported by experimental validation with the goal of investigating the process dynamics of a packed bed reactor taking part in a syngas-based CLC system, as a fuel and air reactor in alternation.

The novelty of the research lies in the modelling work and results. A multiscale 1D model was developed to simulate the reduction and oxidation steps taking place in a CLC process with ilmenite, a titanium-iron oxide, as the oxygen carrier and was validated using breakthrough data published by Gallucci et al. [78]. The model accounts for macroscale interactions in the packed bed, represented by the bed length, a 1D space dimension, as well as interactions at the microscale within the particles, represented by the particle radius, and a 1D space dimension. Modelling work was simplified by only considering the iron component of the OC.

Subsequently, a study of the system dynamics was carried out to examine the effects of varying flow rates, as well as different particle dimensions. Furthermore, a 3D CFD model was developed to study the behaviour of ilmenite particles during the reduction phase of a CLC process, with focus on heat transfer effects.

As a result of validation of the models describing iron-based OC reduction with H_2 and CO, a model simulating ilmenite reduction with syngas was developed.

In order to investigate mass transfer efficiency, normalized concentration was plotted against normalized time in Figure 17. Normalized concentration for H_2 was calculated by dividing concentration at simulation time with inlet concentration, while for CO it was calculated by dividing concentration with

concentration at steady state, after breakthrough (due to carbon deposition). The normalized time was calculated by dividing the simulation time with the time corresponding to a breakthrough point of 0.5.

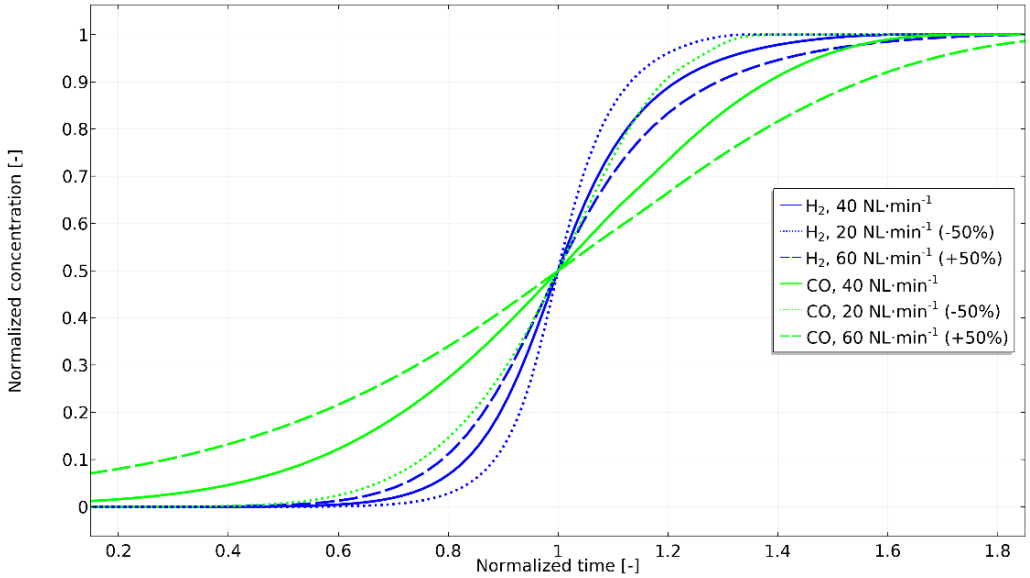

Figure 17. Mass transfer effects following a flow rate sensitivity analysis during reduction with syngas

Assessment of the shape of the breakthrough curves showed steeper profiles at all flow rates for H_2, rather than for CO, meaning faster kinetics, a smaller mass transfer zone, and a higher reaction rate when reducing iron-based OC with H_2, corresponding with findings published by Ortiz et al. [79] on redox kinetics regarding ilmenite granules used in CLC. Finally, with increasing flow rate, the breakthrough profiles lost sharpness, which was expected behaviour.

The effects of particle dimension over mass transfer rate can be seen in Figure 18. The mass of ilmenite OC was identical for all cases; as such, the breakthrough times were also identical. In order to investigate mass transfer efficiency, normalized concentration at the outlet was plotted against normalized time. The sharpest profile for both CO and H_2 was seen when considering the smallest particle dimension due to the shorter diffusion path length inside the particle, leading to suppressing diffusion limitations and maximizing the reduction reaction inside the OC. This then indicates that mass transfer efficiency increased with a decrease in particle size.

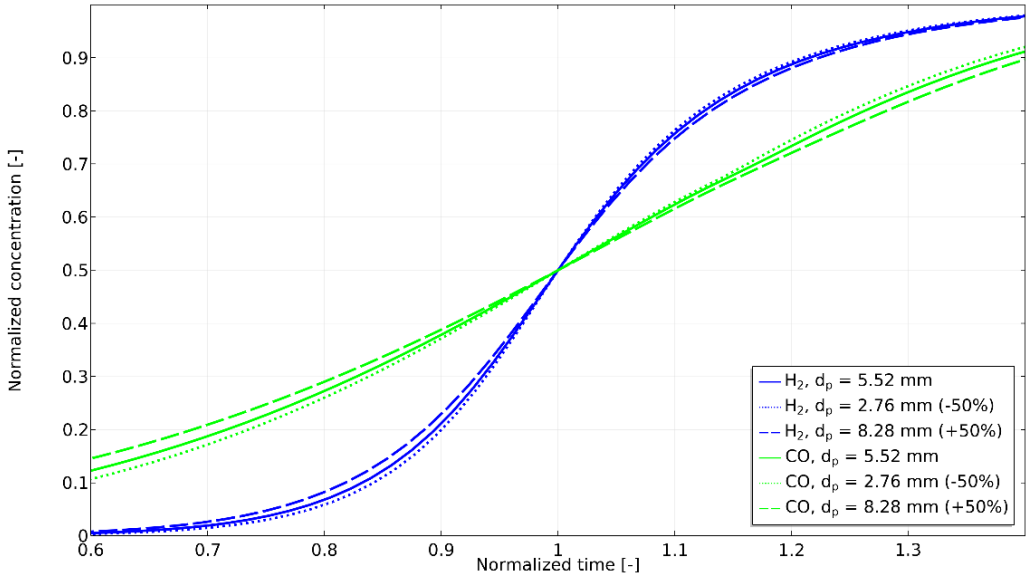

Figure 18. Mass transfer effects following a particle dimension sensitivity analysis during reduction with syngas

Additionally, a 3D CFD particle model was developed to enable a detailed investigation into the reduction step at the microscale level. The model described the reduction reaction using syngas within an ilmenite particle, with equations accounting for mass, heat, and momentum transfer. The individual phenomena involved, as well as the interdependency between them, were studied and discussed. As opposed to the multiscale model which considered a dynamic reactor temperature, but a constant particle temperature, the particle model's complexity led to an accurate description of heat transfer on a microscale level. However, comparison of temperature changes predicted by the models indicated a small difference of just 1 K during the exothermic reduction reaction under identical operating conditions.

4.3. Gasification-based CL systems for hydrogen and power-cogeneration

The investigated IGCC designs with chemical and calcium looping cycles produced about 400 MW - 600 MW net power with a carbon capture rate higher than 90%. A special feature of these concepts, namely hydrogen and power co-generation was also evaluated to assess the possibility of increasing the overall energy conversion efficiency. Several mass and energy integration aspects (i.e., thermal integration of looping cycles in overall steam cycle of the plant, air separation unit - gas turbine air integration, evaluation of various hydrogen-fuelled gas turbines, etc.) were evaluated with the main focus of improving the plant energy efficiency.

The following Shell-based IGCC power plant concepts were evaluated in this work in conjunction with chemical and calcium looping systems used for CO_2 capture:

- Case 1: IGCC without CCS;
- Case 2: IGCC with Selexol-based gas-liquid system for pre-combustion capture;
- Case 3: IGCC with ilmenite-based looping system for pre-combustion capture;
- Case 4: IGCC with calcium-based looping system for pre-combustion capture.

The mass and energy balances derived from modelling and simulations of various plant concepts were used to calculate the key technical and environmental performance indicators of the evaluated IGCC power plant with and without carbon capture. Table 3 presents the main technical and environmental performance indicators for evaluated cases in a power generation scenario.

Table 3. Overall performance indicators for Cases 1 to 4 (power generation only)

Main performance indicator	Unit	Case 1	Case 2	Case 3	Case 4
Coal flow rate (a.r.)	$t \cdot h^{-1}$	152.50	165.70	162.33	226.71
Coal LHV (a.r.)	$MJ \cdot kg^{-1}$	25.353			
Coal thermal energy (A)	MW_{th}	1073.98	1166.97	1143.28	1596.64
Gas turbine power output (M701G2)	MW_e	334.00	334.00	334.00	334.00
Steam turbine power output	MW_e	225.37	210.79	199.45	410.49
Expander power output	MW_e	1.78	0.77	1.50	1.40
Gross electric power output (B)	MW_e	561.15	545.56	534.95	745.89
Ancillary consumption (C)	MW_e	73.89	109.70	96.06	154.74
Net power output (D = B - C)	MW_e	487.26	435.86	438.89	591.15
Gross efficiency (B / A × 100)	%	52.25	46.74	46.79	46.71
Net efficiency (D / A × 100)	%	45.37	37.35	38.38	37.02
Carbon capture rate	%	0.00	90.00	99.55	95.94
CO_2 specific emissions	$kg \cdot MWh^{-1}$	761.87	86.28	3.08	32.89
SPECCA	$MJ \cdot kg^{-1}$	-	2.52	1.90	2.45

As it can be noticed from Table 3, introduction of carbon capture technology implies an energy penalty (in the form of reducing the overall plant energy efficiency). The lowest energy penalty (about 7 net efficiency percentage points) is recorded from Case 3 (ilmenite-based chemical looping cycle) coupled with

an almost total decarbonisation rate (>99%) and the lowest SPECCA value (1.9 MJ/kg). Case 4 (calcium-based looping cycle) has an overall plant net efficiency in the range of 37% (energy penalty for CO_2 capture is about 8.35 net efficiency percentage points), the carbon capture rate is slightly lower (~96%) and has a higher SPECCA value (comparable with Selexol benchmark case). The significantly better performance of Case 3 compared to Case 4 is mainly due to the full combined cycle configuration versus the situation in which some of the coal is introduced in the calcination reactor for sorbent regeneration (single steam cycle) and higher carbon capture capability.

Table 4 presents the main technical and environmental performance indicators for hydrogen and power co-production scenario for Case 3 considered as illustrative example.

Table 4. Overall performance indicators for Case 3 (hydrogen and power co-generation)

Main performance indicator	**Unit**	**Power only**	**Hydrogen and power co-generation**	
Coal flow rate (a.r.)	$t \cdot h^{-1}$		162.33	
Coal LHV (a.r.)	$MJ \cdot kg^{-1}$		25.353	
Coal thermal energy (A)	MW_{th}		1143.28	
Gas turbine power output (M701G2)	MW_e	334.00	293.05	252.10
Steam turbine power output	MW_e	199.45	179.71	158.85
Expander power output	MW_e	1.50	1.46	1.41
Gross electric power output (B)	MW_e	534.95	474.22	412.36
Hydrogen thermal output (C)	MW_{th}	0.00	100.00	200.00
Ancillary consumption (D)	MW_e	96.06	94.52	93.01
Net power output (E = B - D)	MW_e	438.89	379.70	319.35
Net efficiency (E / A × 100)	%	38.38	33.21	27.93
Hydrogen efficiency (C / A × 100)	%	38.38	8.74	17.49
Cumulative energy efficiency	%	38.38	41.95	45.42
Carbon capture rate	%	99.55	99.55	99.55
CO_2 specific emissions (energy)	$kg \cdot MWh^{-1}$	3.08	2.79	2.60

As it can be observed from Table 4, the hydrogen and power co-generation capability has beneficial consequences in increasing cumulative plant energy efficiency and decreasing CO_2 specific emissions. In

addition, as evaluated by Cormos et al. [80], the co-generation scenario has also economic advantages, such as lower specific capital investment costs, better usage of equipment, increased plant flexibility and lower production costs.

As the evaluations showed, the ilmenite-based chemical looping cycle had the highest energy efficiency (about 38.4%) and an almost total decarbonisation rate (>99%), since the calcium-based looping cycle had slightly lower energy efficiency (37%) and carbon capture rate (about 96%), but both looping concepts showed superior performances than the benchmark case (physical gas-liquid absorption using Selexol).

The hydrogen and power co-generation showed a very promising potential in increasing cumulative energy efficiency (up to 45% comparable to the efficiency of the benchmark case without carbon capture) and reducing CO_2 capture energy penalty. ASU-GT air integration was another option to further increase the overall net efficiency by about 1.25 percentage points.

5. Concluding remarks

The research performed in this thesis focused on the evaluation of three gas-solid processes, WGS, SEWGS and CL, used in gas-solid energy conversion systems with carbon capture. The processes were studied by means of process flow diagram design, modelling and simulation, as well as technical and thermal integration aspects.

Chapter 3.1 studied the adsorption step of SEWGS considering novel structured bed reactor configurations, instead of conventional fixed bed reactors, through numerical CFD modelling.

COMSOL Multiphysics was used to develop a 1D CFD model of adsorption for a fixed bed reactor in order to verify the model accuracy against existing studies. Subsequently, 2D CFD simulations were developed to describe adsorption inside monolith structures, both free and porous regions. The multi-component adsorption isotherm used in the simulations was validated with published breakthrough capacities for CO_2 and H_2O at different pressures. Model predictions were in agreement with expected behavior, as monolith reactors provide a more efficient mass transfer. Furthermore, five different longitudinal channel configurations were investigated in terms of mass transfer rate, with model results indicating the high importance of local gas mixing, sorbent distribution and adsorption related heat transfer effects when considering optimal channel design.

Secondly, an evaluation was carried out regarding the accuracy with which the CFD models calculated axial dispersion. The axial dispersion coefficient was estimated from the simulated RTD through the tracer transport method. An acceptable agreement was seen between model predictions and analytically calculated estimations of axial dispersion for different channel shapes. Subsequently, the validated axial dispersion model was used in building 2D and 3D CFD models of adsorption for monolith structures. 3D models were developed considering three different channel shapes: circular, square and hexagonal. The results showed that the differences between the full 3D models and the simplified 2D models were significant in terms of breakthrough times and fluid flow predictions. The difference stemmed from the missing velocity vector in the third coordinate axis for 2D models. For accurate results, it was necessary to consider the full complexity of a 3D geometry, which required heavy computational resources. Most efficient mass transfer was predicted by the 3D hexagonal channel model, even though the breakthrough profiles were similar for all channel shapes due to the low flow rates, laminar flow regime and small channel lengths considered.

Finally, 1D multiscale fixed bed and 3D structured bed models were developed to evaluate mass transfer performance in the adsorption step of SEWGS. The packed bed multiscale CFD model was validated using breakthrough experimental data. A bench-scale CFD structured bed model was developed and validated based on breakthrough measurements performed by TNO using 3D-printed K-HTC monolith

structures. Furthermore, geometry effects on mass transfer efficiency were investigated through CFD modelling for the bench-scale reactor. A scale-up of the monolith model to pilot-scale allowed for a proper comparison with the packed bed technology. Monolith reactor model breakthrough predictions showed there was a considerable increase in mass transfer rate over the packed bed reactor for the adsorption step in SEWGS, as well as an increase in performance (i.e., based on time required for complete sorbent loading) by 23.23% when considering a structured bed configuration, demonstrating promising potential towards enhancing the carbon capture technology.

Chapter 3.2 assessed three WGS process configurations to be applied in catalytic reforming and gasification designs ranging from the conventional designs, such as multiple catalytic shift reactors, to more innovative reactive gas-solid systems (i.e., chemical and calcium looping technologies) for simultaneous syngas conversion and carbon capture. As illustrative examples, the coal gasification for hydrogen and power co-generation with carbon capture were assessed. Based on the evaluations, the reactive gas-solid systems seemed more promising in reducing the energy penalty for CO_2 capture and increasing the overall energy efficiency and carbon capture rate. The looping cycles proved significant advantages compared to conventional design, i.e., higher overall plant energy efficiency by about 0.9 net efficiency points - 1.9 net efficiency points, higher carbon capture rate of 96% - 99% vs. 90% and lower SPECCA values by about 0.4 $MJ \cdot kg^{-1}$ - 0.9 $MJ \cdot kg^{-1}$.

Chapter 4 evaluated chemical looping technologies by undergoing three different methods of investigation.

In Chapter 4.1, a dynamic mathematical model was developed to simulate packed bed reactors used in a methane-based chemical looping combustion process with iron-based oxygen carrier. The air and fuel reactor models were interconnected with the models describing the purge steps of the process to highlight the dynamic behaviour of the entire process. The developed model was used to predict (in space and time): gas flow profile, gas composition distribution, behaviour of oxygen carrier and temperature profiles inside the air and fuel reactors. The simulation results of the 1D model were compared with the experimental data published in the literature. The developed model was able to describe the process very accurately, for a wide range of gas flow rates. A sensitivity study concerning flow rate was performed. Model results showed that increasing the flowrate by 20% of the base value led to a shorter time in which the process achieved stationarity by approximately 300 s (for oxidation step).

A second dynamic mathematical model was developed in order to simulate packed bed reactors used in a CLC process with syngas and iron-based OC. Mass and energy balance equations for the packed bed reactors, together with equations describing the kinetics for the oxidation and reductions steps, were implemented in MATLAB/Simulink. A single gas composition was considered for the oxidation step, while for the reduction step, two different gas compositions were studied. The developed models solved the

equations in space and time and were used to predict gas flow profiles, composition distributions, OC behaviour and temperature profiles during all CLC stages. The validated models could be used for evaluating the behaviour of a dynamic CLC unit, a paramount step in designing a flexible power plant concept.

In Chapter 4.2, a 1D CFD multiscale model was developed to study the reduction and oxidation steps in a syngas-based CLC system and was validated using literature data ($R = 0.99$). In order to investigate mass transfer effects, flow rate and particle dimension studies were carried out. Sharper mass transfer rates were seen at lower flow rates and smaller granule sizes due to suppression of diffusion limitations. In addition, a 3D CFD particle model was developed to investigate in depth the reduction within an ilmenite particle, with focus on heat transfer effects. Minor differences of 1 K were seen when comparing temperature changes predicted by the two models during the slightly exothermic reduction reaction with syngas. The results of the 3D single particle model provided additional understanding regarding influence of mass and heat transfer processes on reduction rate of an iron-based oxygen carrier with syngas.

Finally, an energy integration analysis was carried out in Chapter 4.3, in which several innovative reactive gas-solid systems were assessed in pre-combustion CO_2 capture designs in connection with an IGCC power plant. The most important mass and energy integration issues for a coal-based IGCC plant with innovative chemical and calcium looping systems were evaluated. The designs produced around 400 MW - 600 MW net electricity with a flexible hydrogen output and a carbon capture rate higher than 90%. The principal focus of the work was on the evaluation integration aspects to maximize the overall energy efficiency. Optimization included heat and power integration analysis of main plant sub-systems as well as performing sensitivity analysis. The overall conclusion was that gasification technology coupled with innovative chemical or calcium looping cycles proves to be very promising to deliver high energy efficiency, better operational flexibility simultaneously with very low CO_2 emissions. The ilmenite-based chemical looping cycle had the highest energy efficiency (about 38.4%) and an almost total decarbonisation rate (>99%), since the calcium-based looping cycle had slightly lower energy efficiency (37%) and carbon capture rate (about 96%), but both looping concepts showed superior performances than the benchmark case (physical gas-liquid absorption using Selexol).

The inevitable transition to a new, clean energy economy will be driven by policy action, urgency to combat climate change and the imminent competitiveness of low-carbon technologies brought about by innovation across all sectors (i.e., power, energy efficiency, industry and transportation).

The modelling work presented in this thesis furthers the research into low carbon technologies (i.e., WGS, SEWGS and CL). With the validated CFD models, optimization and design of complex 3D-structured sorbent reactors are possible in order to achieve an increase in SEWGS performance by enhancing adsorption rate through geometry-related mixing effects, while the results of the 3D single

particle model aid in studying mass and heat transport effects on reduction rate of an iron-based oxygen carrier with syngas within CLC. Finally, the various process models shown can help in evaluating which capture technology is most suitable under particular circumstances, at an industrial scale, by carefully tracking KPIs specific to energy conversion systems with and without carbon capture.

References

[1] Le Treut H, Sommerville R, Cubasch U, Ding Y, Mauritzen C, Mokssit A, et al. Historical Overview of Climate Change Science. Cambridge, UK and New York, NY, USA, 95-122: In: Climate change 2007: the physical science basis. Contribution of Working Group I to the Fourth Assessment Report of the Intergovernmental Panel on Climate Change, Cambridge University Press; 2007.

[2] IPCC. Climate Change 2014: Synthesis Report. Contribution of Working Groups I, II and III to the Fifth Assessment Report of the Intergovernmental Panel on Climate Change. 2014.

[3] World Resources Institute. World Greenhouse Gas Emissions 2016 n.d. https://www.wri.org/data/world-greenhouse-gas-emissions-2016 (accessed October 3, 2021).

[4] IPCC. Climate Change 2014: Mitigation of Climate Change. Contribution of Working Group III to the Fifth Assessment Report of the Intergovernmental Panel on Climate Change. 2014.

[5] United States Environmental Protection Agency. Global Greenhouse Gas Emissions Data n.d. https://www.epa.gov/ghgemissions/global-greenhouse-gas-emissions-data (accessed October 3, 2021).

[6] IEA. Energy Technology Perspectives 2017: Catalysing Energy Technology Transformations. Paris: 2017.

[7] World Steel Association. Steel's contribution to a low carbon future and climate resilient socities - Worldsteel position paper. 2017.

[8] IEA. Tracking Industry 2020: Chemicals. Paris: 2020.

[9] IEA. Tracking Industry 2020: Aluminium. Paris: 2020.

[10] IEA. Global Energy Review 2021. Paris: 2021.

[11] Global CCS Institute. The Global Status of CCS Report 2018. Australia: 2018.

[12] EIA. World Energy Outlook 2011. Washington, DC, USA: 2011.

[13] Global CCS Institute. The Global Status of CCS Report 2020. 2020.

[14] IPCC. Carbon Dioxide Capture and Storage Report. Prepared by Working Group III of the Intergovernmental Panel on Climate Change. Cambridge, England: 2005.

[15] Meuleman E, Cottrell A, Ghayur A. Treatment of flue-gas impurities for liquid absorbent-based post-combustion CO2 capture processes. Absorption-Based Post-Combustion Capture of Carbon Dioxide 2016:519–51. https://doi.org/10.1016/B978-0-08-100514-9.00022-6.

[16] Mostafavi E, Ashrafi O, Navarri P. Assessment of process modifications for amine-based post-combustion carbon capture processes. Clean Eng Technol 2021;4:100249. https://doi.org/10.1016/J.CLET.2021.100249.

[17] Espatolero S, Romeo LM. Optimization of Oxygen-based CFBC Technology with CO2 Capture. Energy Procedia 2017;114:581–8. https://doi.org/10.1016/J.EGYPRO.2017.03.1200.

[18] Chein R, Chen YC, Chung JN. Numerical study of methanol–steam reforming and methanol–air catalytic combustion in annulus reactors for hydrogen production. Appl Energy 2013;102:1022–34. https://doi.org/10.1016/J.APENERGY.2012.06.010.

[19] Chen WH, Shen CT, Lin BJ, Liu SC. Hydrogen production from methanol partial oxidation over Pt/Al2O3 catalyst with low Pt content. Energy 2015;88:399–407. https://doi.org/10.1016/J.ENERGY.2015.05.055.

[20] Pasel J, Samsun RC, Tschauder A, Peters R, Stolten D. A novel reactor type for autothermal reforming of diesel fuel and kerosene. Appl Energy 2015;150:176–84. https://doi.org/10.1016/J.APENERGY.2015.04.038.

[21] Lu X, Wang T. Water–gas shift modeling in coal gasification in an entrained-flow gasifier – Part 2: Gasification application. Fuel 2013;108:620–8. https://doi.org/10.1016/J.FUEL.2013.02.024.

[22] Wang L, Fang D, Huang X, Zhang S, Qi Y, Liu Z. Influence of Reaction Conditions on Methanol Synthesis and WGS Reaction in the Syngas-to-DME Process. J Nat Gas Chem 2006;15:38–44. https://doi.org/10.1016/S1003-9953(06)60005-4.

[23] Van Der Laan GP, Beenackers AACM. Intrinsic kinetics of the gas–solid Fischer–Tropsch and water gas shift reactions over a precipitated iron catalyst. Appl Catal A Gen 2000;193:39–53. https://doi.org/10.1016/S0926-860X(99)00412-3.

[24] Chen WH, Lin MR, Yu AB, Du SW, Leu TS. Hydrogen production from steam reforming of coke oven gas and its utility for indirect reduction of iron oxides in blast furnace. Int J Hydrogen Energy 2012;37:11748–58. https://doi.org/10.1016/J.IJHYDENE.2012.05.021.

[25] Reddy GK, Smirniotis PG. Water Gas Shift Reaction: Research Developments and Applications. Elsevier; 2015.

[26] Chen WH, Chiu TW, Hung CI. Hysteresis loops of methane catalytic partial oxidation for hydrogen production under the effects of varied Reynolds number and Damköhler number. Int J Hydrogen Energy 2010;35:6291–302. https://doi.org/10.1016/J.IJHYDENE.2010.03.133.

[27] Meng L, Tsuru T. Microporous Silica Membrane Reactors. Curr Trends Futur Dev Membr Microporous Membr Membr React 2019:127–56. https://doi.org/10.1016/B978-0-12-816350-4.00006-4.

[28] van Selow ER, Cobden PD, van den Brink RW, Hufton JR, Wright A. Performance of sorption-enhanced water-gas shift as a pre-combustion CO_2 capture technology. Energy Procedia 2009;1:689–96. https://doi.org/10.1016/J.EGYPRO.2009.01.091.

[29] Szima S, Arnaiz del Pozo C, Cloete S, Chiesa P, Jiménez Alvaro Á, Cormos AM, et al. Finding synergy between renewables and coal: Flexible power and hydrogen production from advanced IGCC plants with integrated CO2 capture. Energy Convers Manag 2021;231:113866. https://doi.org/10.1016/J.ENCONMAN.2021.113866.

[30] van Selow ER, Cobden PD, Wright AD, van den Brink RW, Jansen D. Improved sorbent for the sorption-enhanced water-gas shift process. Energy Procedia 2011;4:1090–5. https://doi.org/10.1016/j.egypro.2011.01.159.

[31] Boon J, Coenen K, van Dijk E, Cobden P, Gallucci F, van Sint Annaland M. Sorption-Enhanced Water–Gas Shift. Adv Chem Eng 2017;51:1–96. https://doi.org/10.1016/BS.ACHE.2017.07.004.

[32] Ebner AD, Reynolds SP, Ritter JA. Understanding the adsorption and desorption behavior of CO_2 on a K-promoted hydrotalcite-like compound (HTlc) through nonequilibrium dynamic isotherms. Ind Eng Chem Res 2006;45:6387–92. https://doi.org/10.1021/ie060389k.

[33] Walspurger S, Cobden PD, Safonova OV, Wu Y, Anthony EJ. High CO_2 storage capacity in alkali-promoted hydrotalcite-based material: In situ detection of reversible formation of magnesium carbonate. Chem – A Eur J 2010;16:12694–700. https://doi.org/10.1002/chem.201000687.

[34] Yong Z, Rodrigues AE. Hydrotalcite-like compounds as adsorbents for carbon dioxide. Energy Convers Manag 2002;43:1865–76. https://doi.org/10.1016/S0196-8904(01)00125-X.

[35] Lee KB, Beaver MG, Caram HS, Sircar S. Reversible chemisorbents for carbon dioxide and their potential applications. Ind Eng Chem Res 2008;47:8048–62. https://doi.org/10.1021/ie800795y.

[36] Boon J, Cobden PD, van Dijk HAJ, van Sint Annaland M. High-temperature pressure swing

adsorption cycle design for sorption-enhanced water-gas shift. Chem Eng Sci 2015;122:219–31. https://doi.org/10.1016/J.CES.2014.09.034.

[37] Van Selow ER, Cobden PD, Verbraeken PA, Hufton JR, Van Den Brink RW. Carbon capture by sorption-enhanced water-gas shift reaction process using hydrotalcite-based material. Ind Eng Chem Res 2009;48:4184–93. https://doi.org/10.1021/ie801713a.

[38] Jansen D, Van Selow E, Cobden P, Manzolini G, Macchi E, Gazzani M, et al. SEWGS Technology is Now Ready for Scale-up! Energy Procedia 2013;37:2265–73. https://doi.org/10.1016/J.EGYPRO.2013.06.107.

[39] Breeze P. Carbon Capture and Storage. Coal-Fired Gener 2015:73–86. https://doi.org/10.1016/B978-0-12-804006-5.00013-7.

[40] Voitic G, Pichler B, Basile A, Iulianelli A, Malli K, Bock S, et al. Hydrogen Production. Fuel Cells Hydrog From Fundam to Appl Res 2018:215–41. https://doi.org/10.1016/B978-0-12-811459-9.00010-4.

[41] Vozniuk O, Tanchoux N, Millet JM, Albonetti S, Di Renzo F, Cavani F. Spinel Mixed Oxides for Chemical-Loop Reforming: From Solid State to Potential Application. Stud Surf Sci Catal 2019;178:281–302. https://doi.org/10.1016/B978-0-444-64127-4.00014-8.

[42] Fernández-Arévalo T, Lizarralde I, Grau P, Ayesa E. New systematic methodology for incorporating dynamic heat transfer modelling in multi-phase biochemical reactors. Water Res 2014;60:141–55. https://doi.org/10.1016/J.WATRES.2014.04.034.

[43] Chisalita DA, Cormos AM. Dynamic simulation of fluidized bed chemical looping combustion process with iron based oxygen carrier. Fuel 2018;214:436–45. https://doi.org/10.1016/j.fuel.2017.11.025.

[44] Lyngfelt A, Leckner B, Mattisson T. A fluidized-bed combustion process with inherent CO2 separation; application of chemical-looping combustion. Chem Eng Sci 2001;56:3101–13. https://doi.org/10.1016/S0009-2509(01)00007-0.

[45] Pröll T. Fundamentals of chemical looping combustion and introduction to CLC reactor design. Calcium Chem Looping Technol Power Gener Carbon Dioxide (CO 2015:197–219. https://doi.org/10.1016/B978-0-85709-243-4.00010-0.

[46] Speight JG. Types of gasifier for synthetic liquid fuel production: design and technology. Gasif Synth Fuel Prod Fundam Process Appl 2015:29–55. https://doi.org/10.1016/B978-0-85709-802-

3.00002-3.

[47] Noorman S, van Sint Annaland M, Kuipers H. Packed Bed Reactor Technology for Chemical-Looping Combustion. Ind Eng Chem Res 2007;46:4212–20.

[48] Mattisson T, Keller M, Linderholm C, Moldenhauer P, Rydén M, Leion H, et al. Chemical-looping technologies using circulating fluidized bed systems: Status of development. Fuel Process Technol 2018;172:1–12. https://doi.org/10.1016/J.FUPROC.2017.11.016.

[49] Miller BG. Emerging Technologies for Reduced Carbon Footprint. Clean Coal Eng Technol 2017:669–89. https://doi.org/10.1016/B978-0-12-811365-3.00014-4.

[50] Fennel P. Calcium and chemical looping technology: an introduction. Calcium Chem. Looping Technol. Power Gener. Carbon Dioxide Capture, London, UK: Woodhead Publishing; 2015.

[51] Masoudi Soltani S, Lahiri A, Bahzad H, Clough P, Gorbounov M, Yan Y. Sorption-enhanced Steam Methane Reforming for Combined CO2 Capture and Hydrogen Production: A State-of-the-Art Review. Carbon Capture Sci Technol 2021;1:100003. https://doi.org/10.1016/J.CCST.2021.100003.

[52] Bohn CD, Müller CR, Cleeton PJ, Hayhurst NA, Davidson FJ, Scott AS, et al. Production of Very Pure Hydrogen with Simultaneous Capture of Carbon Dioxide using the Redox Reactions of Iron Oxides in Packed Beds. Ind Eng Chem Res 2008;47:7623–30.

[53] Hydrogen Council. Hydrogen scaling up: A sustainable pathway for the global energy transition. 2017.

[54] International Renewable Energy Agency (IRENA). Hydrogen: A renewable energy perspective. Abu Dhabi: 2019.

[55] Frischmuth F, Härtel P. Hydrogen sourcing strategies and cross-sectoral flexibility trade-offs in net-neutral energy scenarios for Europe. Energy 2022;238:121598. https://doi.org/10.1016/J.ENERGY.2021.121598.

[56] Colbertaldo P, Agustin SB, Campanari S, Brouwer J. Impact of hydrogen energy storage on California electric power system: Towards 100% renewable electricity. Int J Hydrogen Energy 2019;44:9558–76. https://doi.org/10.1016/J.IJHYDENE.2018.11.062.

[57] IEA. The Future of Hydrogen. Paris: 2019.

[58] IEA. Hydrogen. 2020.

[59] International Energy Agency. Transforming Industry through CCUS. 2019.

[60] Manzolini G, Giuffrida A, Cobden PD, van Dijk HAJ, Ruggeri F, Consonni F. Techno-economic assessment of SEWGS technology when applied to integrated steel-plant for CO2 emission mitigation. Int J Greenh Gas Control 2020;94:102935. https://doi.org/10.1016/j.ijggc.2019.102935.

[61] Alalwan HA, Alminshid AH. CO2 capturing methods: Chemical looping combustion (CLC) as a promising technique. Sci Total Environ 2021;788:147850. https://doi.org/10.1016/J.SCITOTENV.2021.147850.

[62] MathWorks. Simulink: User Guide. 2021.

[63] MathWorks. S-function callback methods n.d. https://www.mathworks.com/help/simulink/sfg/s-function-callback-methods.html (accessed October 24, 2021).

[64] Eshkabilov SL. Practical MATLAB Modeling with Simulink: Programming and Simulating Ordinary and Partial Differential Equations. 1st editio. New York, US: Apress; 2020.

[65] COMSOL. COMSOL Multiphysics Documentation. 2021.

[66] Chemstations. CHEMCAD: User Guide. 2021.

[67] Yu H, Vikse M, Gundersen T. Comparison of reformulations of the Duran-Grossmann model for Work and Heat Exchange Network (WHEN) synthesis. Comput Aided Chem Eng 2018;43:489–94. https://doi.org/10.1016/B978-0-444-64235-6.50087-5.

[68] Roetzel W, Luo X, Chen D. Optimal design of heat exchanger networks. Des Oper Heat Exch Their Networks 2020:231–317. https://doi.org/10.1016/B978-0-12-817894-2.00006-6.

[69] Zoughaib A. Energy Integration of Continuous Processes: From Pinch Analysis to Hybrid Exergy/Pinch Analysis. From Pinch Methodol to Energy Integr Flex Syst 2017:1–53. https://doi.org/10.1016/b978-1-78548-194-9.50001-6.

[70] Cormos CC, Cormos AM, Petrescu L. Assessment of chemical looping-based conceptual designs for high efficient hydrogen and power co-generation applied to gasification processes. Chem Eng Res Des 2014;92:741–51. https://doi.org/10.1016/J.CHERD.2013.08.023.

[71] Saeidi S, Fazlollahi F, Najari S, Iranshahi D, Klemeš JJ, Baxter LL. Hydrogen production: Perspectives, separation with special emphasis on kinetics of WGS reaction: A state-of-the-art review. J Ind Eng Chem 2017;49:1–25. https://doi.org/10.1016/J.JIEC.2016.12.003.

[72] Cormos AM, Dinca C, Petrescu L, Andreea Chisalita D, Szima S, Cormos CC. Carbon capture and utilisation technologies applied to energy conversion systems and other energy-intensive industrial applications. Fuel 2018;211:883–90. https://doi.org/10.1016/J.FUEL.2017.09.104.

[73] IEAGHG. Potential for improvement in gasification combined cycle power generation with CO2 capture. 2003.

[74] NETL. Cost and performance baseline for fossil energy plants - Volume 1: Bituminous coal and natural gas to electricity. 2010.

[75] Zohrabian A, Mansouri Majoumerd M, Soltanieh M, Sattari S. Techno-economic evaluation of an integrated hydrogen and power co-generation system with CO2 capture. Int J Greenh Gas Control 2016;44:94–103. https://doi.org/10.1016/J.IJGGC.2015.11.004.

[76] van der Spek M, Roussanaly S, Rubin ES. Best practices and recent advances in CCS cost engineering and economic analysis. Int J Greenh Gas Control 2019;83:91–104. https://doi.org/10.1016/J.IJGGC.2019.02.006.

[77] Cormos AM, Cormos CC. Techno-economic assessment of combined hydrogen & power co-generation with carbon capture: The case of coal gasification. Appl Therm Eng 2019;147:29–39. https://doi.org/10.1016/J.APPLTHERMALENG.2018.10.064.

[78] Gallucci F, Hamers HP, van Zanten M, van Sint Annaland M. Experimental demonstration of chemical-looping combustion of syngas in packed bed reactors with ilmenite. Chem Eng J 2015;274:156–68. https://doi.org/10.1016/j.cej.2015.03.081.

[79] Ortiz M, Gallucci F, Snijkers F, Van Noyen J, Louradour E, Tournigant D, et al. Development and testing of ilmenite granules for packed bed chemical-looping combustion. Chem Eng J 2014;245:228–40. https://doi.org/10.1016/J.CEJ.2014.02.030.

[80] Cormos AM, Dinca C, Cormos CC. Multi-fuel multi-product operation of IGCC power plants with carbon capture and storage (CCS). Appl Therm Eng 2015;74:20–7. https://doi.org/10.1016/J.APPLTHERMALENG.2013.12.080.